Dynamic Control of Microbial Movement by Photoswitchable ATP Antagonists

（光応答性ATPアンタゴニストによる微生物の運動の可逆的制御）

A Thesis

Submitted for the Degree of

Doctor of Life Science

By

Sampreeth Thayyil

Laboratory of Smart Molecules

Transdisciplinary Life Science Course

Graduate School of Life Science

Hokkaido University, Japan

June 2022

DECLARATION

I hereby declare that the matter embodied in this thesis entitled **"Dynamic control of microbial movement by photoswitchable ATP antagonists**" is the result of investigations carried out by me under the supervision of **Prof. Nobuyuki Tamaoki** at the Laboratory of Smart Molecules, Transdisciplinary Life Science Course, Graduate School of Life Science, Hokkaido University, Japan, and it has not been submitted elsewhere for the award of any degree or diploma.

In keeping with the general practice of reporting scientific observations, due acknowledgement has been made whenever the work described has been based on the findings of the other investigators. Any omission that might have occurred by oversight or error of judgments is regretted.

Sampreeth Thayyil

CERTIFICATE

I hereby certify that the work described in this thesis entitled "**Dynamic control of microbial movement by photoswitchable ATP antagonists"** has been carried out by **Sampreeth Thayyil**, under the supervision of **Prof. Nobuyuki Tamaoki** at the Laboratory of Smart Molecules, Transdisciplinary Life Science Course, Graduate School of Life Science, Hokkaido University, Japan.

Prof. Nobuyuki Tamaoki

(Research Supervisor)

Dedicated to my parents and teachers

Table of contents

Chapter 1
General Introduction

The biological cell consists of many sophisticated nanomachines that perform the complex cellular functions[1]. One category of these nanomachines is classified as "motor proteins" that harness the chemical energy from ATP hydrolysis to generate mechanical motion in a highly efficient manner. Importantly, the motile activity of motor proteins is crucial to perform various biological motion such as movement of organelle, cells and even contribute to the collective motion in some animals[2-4]. Especially, the linear motor proteins kinesin, myosin and dynein are important for maintaining the cellular functions. Kinesin[5] mainly involves in the intracellular cargo transport along microtubules from the center of the cell to the periphery. Myosin[6] motion along the actin filaments is responsible for the muscle contraction and cell migration. Dynein[7] motion towards the minus-end of microtubules results in the retrograde transport of intracellular cargos, cell division and also power in the beating motion of cilia and flagella of microorganisms (Scheme 1).

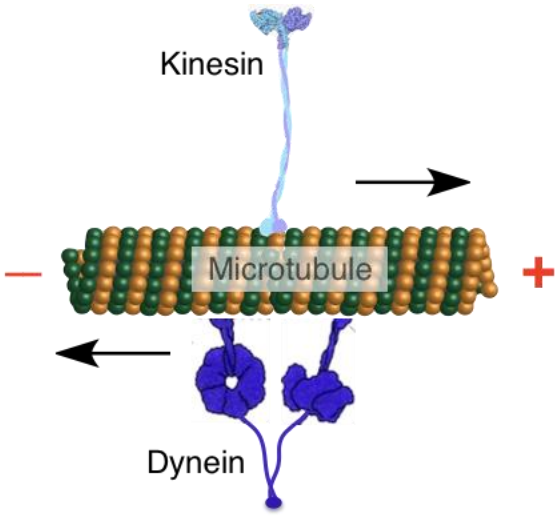

Scheme 1: Representation of the motion of kinesin and dynein towards plus (+) and minus (–) end of microtubule, respectively.

The motor proteins and their unparallel functions also inspired material scientists, which leads to the fabrication of nano-micro mechanical devices for several applications[8,9]. Also, due to its

dysfunction associated with various diseases, motor protein has been considered as one of the drug targets in the development of new drugs[10,11]. Either for biomaterials or for biological application, controlling the motion is extremely challenging. If we achieve such control in a molecular precision level, many potential applications can be realized. Among the different strategies investigated, light responsive molecules offer a highly spatiotemporal control over the activity of biological systems[12]. Photoirradiation of caged ATP[13] and caged inhibitors[14] to switch the motility from OFF to ON, and *vice versa* were the initial studies in this field, but it offers only one-way regulation. This drawback of irreversibility can be replaced by the incorporation of reversible photoswitches for modulating the activity of biological process[15]. Azobenzene has proved to be a robust photoswitch which undergoes reversible photoisomerization with the picosecond time scale without any side products (Scheme 2).

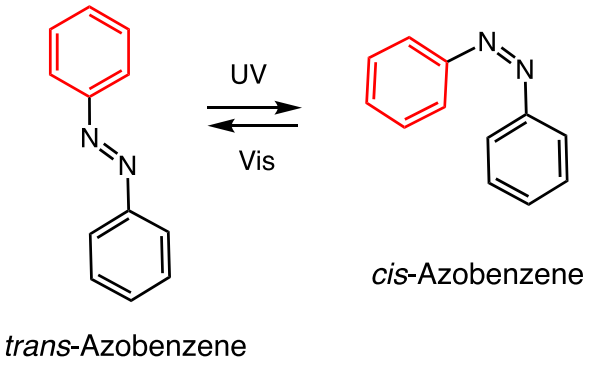

Scheme 2: Representation of *trans-cis* isomerization of azobenzene.

In recent past, our group has reported azobenzene based photo-responsive ATP analog, AzoTP, fuels the kinesin and myosin motor with photo-tunable velocity[16-18]. AzoTP in its *trans* state can power the motion of microtubule and actin filaments on a kinesin or myosin-coated substrate, while the *cis* state can't. Importantly, we have demonstarted the photocontrol of a macroscopic

action through photocontrol of glycerinated skeletal muscle fibre. Next challenge is to apply our concept in actual biological system in an organism/animal level.

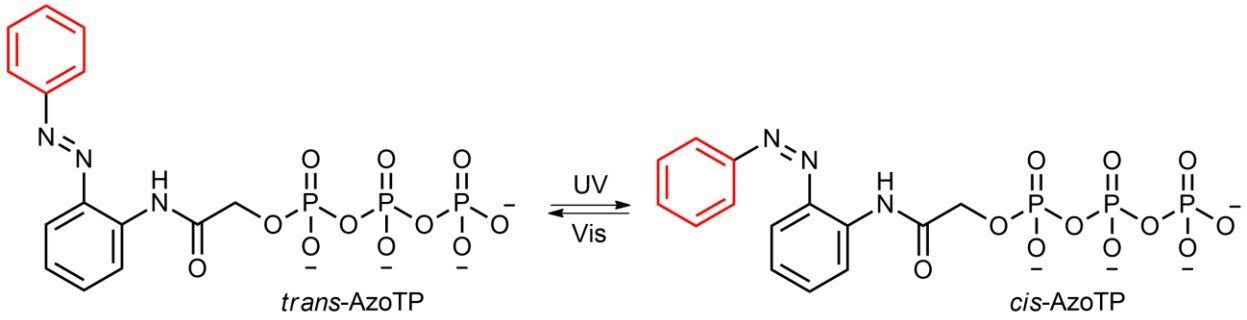

Scheme 3: Representation of *trans-cis* photoisomerization of azobenzene appended ATP analogue (AzoTP).

In this dissertation, the author describes the development of azobenzene-based photoswitchable ATP antagonists for controlling the activity of complex motor proteins in cytoplasmic and axonemal dyneins in an organism level. The dynein motor protein is a suitable candidate for my study because flagella and cilia act as a propeller for the motion of unicellular organisms in an aqueous environment through repeated bending motion obtained by sliding the linear array of axonemal dyneins (inner and outer dynein arms) along the 9+2 pair of microtubules accompanied by hydrolyzing ATP[19-21]. In contrast to the previous observation of AzoTP-triggered gliding motion of microtubules or actin filaments on kinesin or myosin filaments-coated glass surface, respectively, AzoTP did not trigger microtubule gliding motion with dynein. Through detailed investigation we found that AzoTP act as an ATP antagonist in microtubule-dynein system. Interestingly, AzoTP, in the presence of dynein exhibited a higher hydrolysis activity than ATP. Based on these results, the author designed non-hydrolysable analogue of AzoTP, Azo-Amide-PCP and Azo-Propyl-PCP with “amide” and “propyl” spacer between azobenzene (Azo) and

methylene diphosphate (PCP) moieties to work as photoresponsive ATP antagonists. The new ATP antagonists showed reversible photoswitching of cytoplasmic dynein activity in an *in vitro* dynein-microtubule system due to the *trans* and *cis* photoisomerization of their azobenzene segment. Importantly, the new ATP antagonists reversibly regulated the axonemal dynein motor activity for the force generation in a demembranated model of *Chlamydomonas reinhardtii*. The photoresponsive change in the motor activity is well explained by molecular docking studies and found that the *trans* and *cis* isomers of ATP antagonists significantly differ in their affinity to the ATP binding site.

References

[1] M.G.L. Van den Heuvel, C. Dekker, *Science.*, **2007**, *317*, 333-336.

[2] M.Schilwa, G.Woehlke, *Nature*., **2003**, *422*, 759-765.

[3] R. D. Vale and R. A. Milligan, *Science.*, **2000**, *288*, 88-95.

[4] G. Saper, H. Hess, *Chem. Rev*., **2020**, *120*, 288−309.

[5] R.D Vale, T.S. Reese, M.P. Sheetz, *Cell*., **1985**, *42*,39-50.

[6] V. Mermall, P.L. Post, M.S. Mooseker, Science., **1998**, *279*, 527-533.

[7] P. Höök and R. B. Vallee, *J. Cell Sci.*, **2006**, *119*, 4369–4371.

[8] A. Goel and V.Vogel, *Nat. Nanotechnol*., **2008**, *3*, 465-475.

[9] S. Aoyama, M.Shimoike and Y. Hiratsuka, *Proc. Natl. Acad. Sci. U.S.A.*, **2013**, *110*, 16408-16413.

[10] J. M. Gerdes and N. Katsanis, *Cell. Mol. Life Sci*., **2005**, *62*, 1556–1570.

[11] B.A Chabner, T.G. Roberts, *Nat. Rev. Cancer*., **2005**, *5*, 65.

[12] G. Mayer, A. Hechel, *Angew. Chemie-Int.Ed,*, **2006**, *45*, 4900-4921.

[13] H.Higuchi, E. Muto, Y. Inoue, T. Yanagida, *Proc. Natl. Acad. Sci. U.S.A.*, **1997**,*94*, 4395-4400.

[14] A. Nomura, T. Q. P. Uyeda, N. Yumoto and Y. Tatsu, *Chem. Commun*., **2006**, *1*, 3588–3590.

[15] J. M. Beierle, H. A. V Kistemaker, W. A. Velema and B. L. Feringa, *Chem. Rev*., **2013**, *113*, 8, 6114–6178.

[16] N. Perur, M. Yahara, T. Kamei, N. Tamaoki, *Chem. Commun.*, **2013**, *49*, 9935–9937.

[17] H. M. Menezes, M. J. Islam, M. Takahashi, N. Tamaoki, *Org. Biomol. Chem.*, **2017**, *15*, 8894–8903.

[18] M. J. Islam, K. Matsuo, H. M. Menezes, M. Takahashi, H. Nakagawa, A. Kakugo, K. Sada, N. Tamaoki, *Org. Biomol. Chem.*, **2019**, *17*, 53–65.

[19] C. B. Lindemann and K. A. Lesich, *J. Cell Sci.*, **2010**, *123*, 519–528.

[20] S. Toba, H. Iwamoto, S. Kamimura and K. Oiwa, *Biophys. J.*, **2015**, *108*, 2843–2853.

[21] O. Kagami and R. Kamiya, *J. Cell Sci.*, **1992**, *103*, 653–664.

Chapter 2

Dynamic control of microbial movement by photoswitchable ATP antagonists

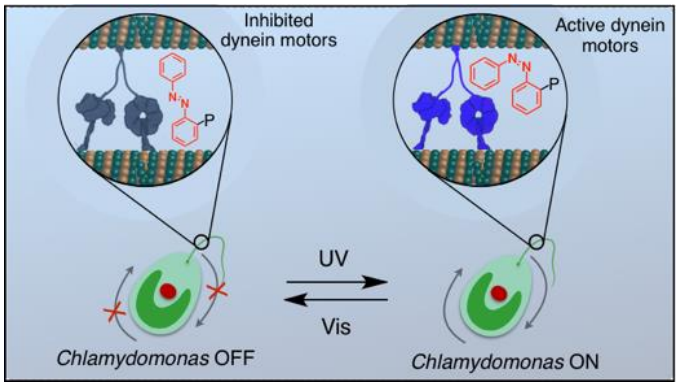

2.1 Introduction

ATP, the "high energy molecule" is essential for all of the living things.[1] In biology, the energy released by ATP hydrolysis is supplied for synthesizing biomacromolecules, various cellular functions, muscle contraction, blood circulation, extracellular signaling, cargo transportation and locomotion of microorganism. [2–4] For instance, motor proteins such as kinesin, myosin and dynein utilize chemical energy from ATP hydrolysis to generate mechanical motion as a prerequisite for various cellular tasks.[5] Due to consumption at a high rate in diseased site such as tumor microenvironment, ATP is also considered as one of the possible targets for cancer therapy.[6,7] Hence, the development of molecular entities that can work as "ATP antagonist" has enormous possibilities in controlling the biochemical processes as well as in designing drugs. Additionally, by appending a stimuli-responsive motif to such ATP antagonist can potentially leads to the regulation of biological processes in a spatiotemporal manner. However, molecules that satisfy structural similarity to ATP together with stimuli-responsivity is extremely challenging to design.

Herein I show azobenzene-based ATP antagonists that respond to light irradiation via *trans* to *cis* isomerization reversibly.[8–14] The ATP antagonist binds to the receptor only in one of the isomer states (*trans*), thus can function as photoswitchable ATP antagonist. I demonstrate biological significance of photoswitchable ATP antagonists using dynein motor protein. Dynein is a cytoskeletal motor protein forming a large complex of 1-2 MDa and exists in two isoforms: cytoplasmic and axonemal dyneins.[15–17] There are multiple ATP binding sites in dynein and the hydrolysis of bound ATP can induce mechanical stepping motion towards the minus-end of microtubules.[18–20] Utilizing ATP energy, cytoplasmic dynein transports intracellular cargos,[21, 22] while axonemal dynein drives the beating motion of flagella and cilia.[23, 24] With the

photoswitchable ATP antagonist, the author show an unprecedented photocontrol of both cytoplasmic and axonemal dyneins using a dynein-microtubule system and a demembranated *Chlamydomonas reinhardtii* model, respectively.

2.2 Results and Discussion

2.2.1 Synthesis and photophysical studies of Azo-triphosphates

I synthesized photoresponsive ATP antagonists (Figure 1a), AzoTP, Azo-Amide-PCP and Azo-Propyl-PCP according to the procedures described in the Experimental section and characterized unambiguously using a variety of analytical methods (HPLC, NMR, Mass) Figure 1-8 (Experimental section). AzoTP, a hydrolysable analogue of ATP, has previously shown to power kinesin and myosin motor proteins in a photoswitchable manner.[25–27] Azo-Amide-PCP and Azo-Propyl-PCP with "amide" and "propyl" spacer between azobenzene (Azo) and methylene diphosphate (PCP) moieties were newly designed non-hydrolysable analogues of ATP. Photoswitching ability of ATP antagonists was studied by using absorption spectroscopy in BRB80 buffer (pH 6.9) (Figure 2).[28,29] As synthesized *trans* isomers of these ATP antagonists exhibited two absorption bands (λ_{max} = ~327 nm and 430 nm) assignable for π-π* and n-π* electronic transitions, respectively. Upon 365 nm light irradiation, the intensity of absorption bands was significantly altered to reach a UV photostationary state (UV_{PSS}) (Figure 2) containing 92% (Azo-Amide-PCP) and 88% (Azo-Propyl-PCP) *cis* isomer (determined by ^{1}H NMR in Figure 3 and Table 1). Upon 430 nm light irradiation (Vis_{PSS}), an opposite trend in the change of absorption bands containing 72% (Azo-Amide-PCP) and 75% (Azo-Propyl-PCP) *trans* isomer was observed. As shown in Figure 2b, d, the compounds (Azo-Amide-PCP and Azo-Propyl-PCP) underwent

reversible *trans-cis* photoisomerization for at least five cycles without significant fatigue. Thermal relaxation lifetimes for *cis* isomers in the compounds were >3 days at 25 °C (Figure 4).

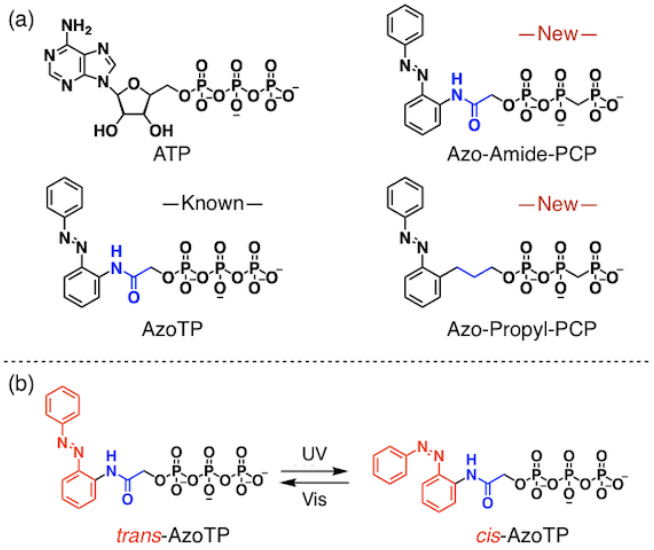

Figure 1. (a) Molecular structures of ATP and ATP antagonists, AzoTP, Azo-Amide-PCP and Azo-Propyl-PCP. (b) Scheme showing the *trans* to *cis* isomerization of AzoTP by UV and Vis light irradiations.

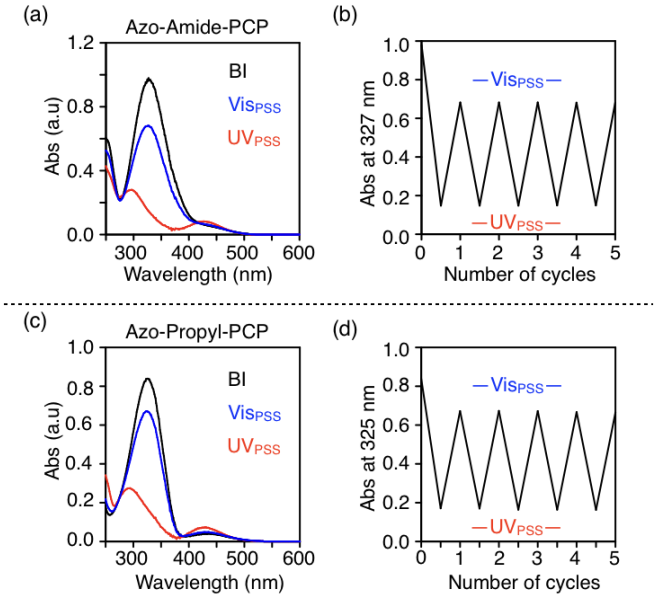

Figure 2. UV-Visible absorption spectra of Azo-Amide-PCP (6.1 x10^{-4} M) (a) and Azo-Propyl-PCP (5 x 10^{-4} M) (c) in BRB-80 buffer at 25 °C before irradiation (BI, black line), photo-stationary state of UV (UVPSS, red line) and Vis (VisPSS, blue line) irradiations. Absorbance changes at λmax obtained by repeated irradiation (5 cycles) at UVPSS and VisPSS (c and d).

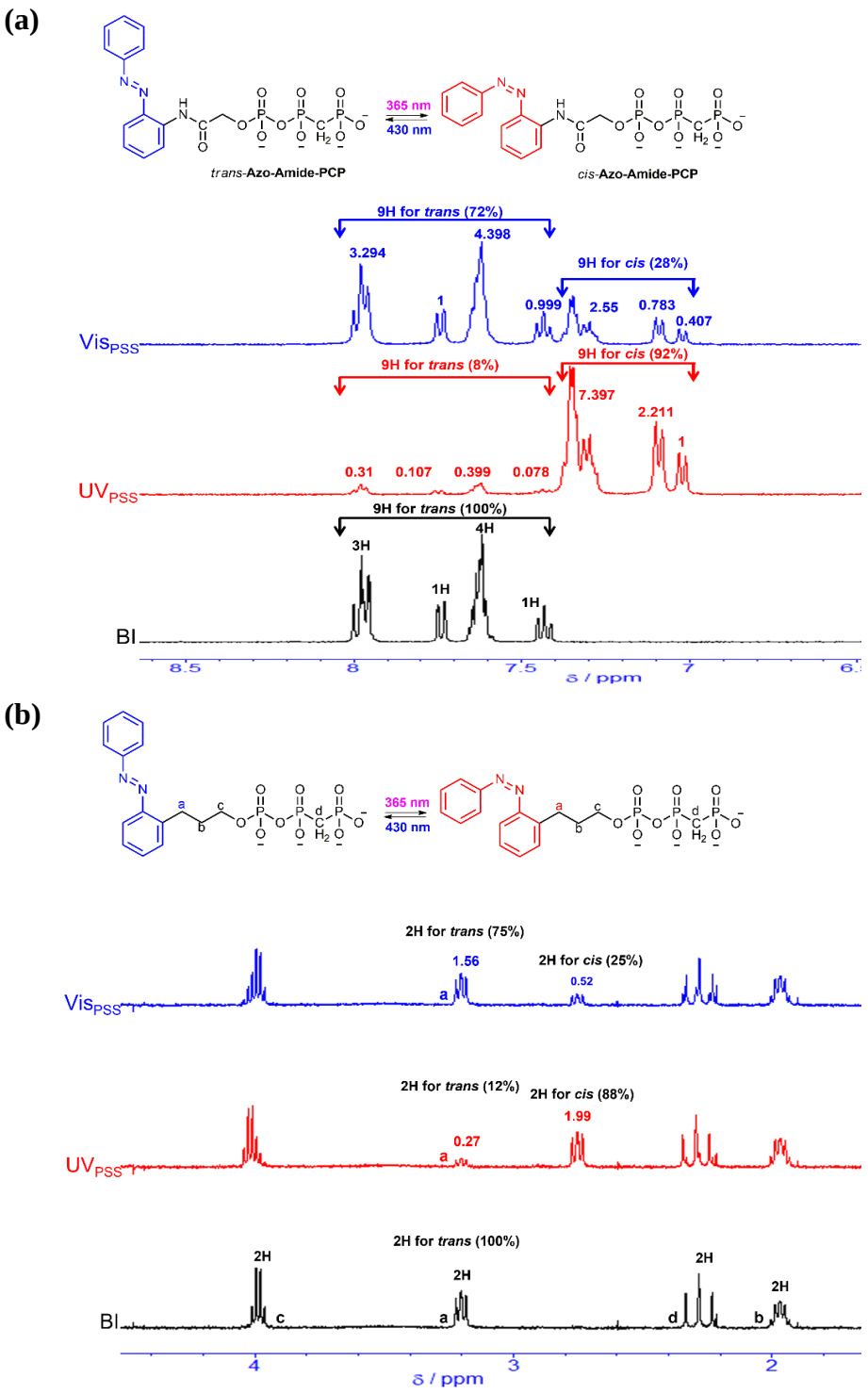

Figure 3. ^{1}H NMR (400 MHz, D_2O) showing the *cis*/*trans* isomer ratios of (a) Azo-Amide-PCP, (b) Azo-Propyl-PCP at before irradiation (BI), UV_{PSS} (365nm) and Vis_{PSS} (430nm).

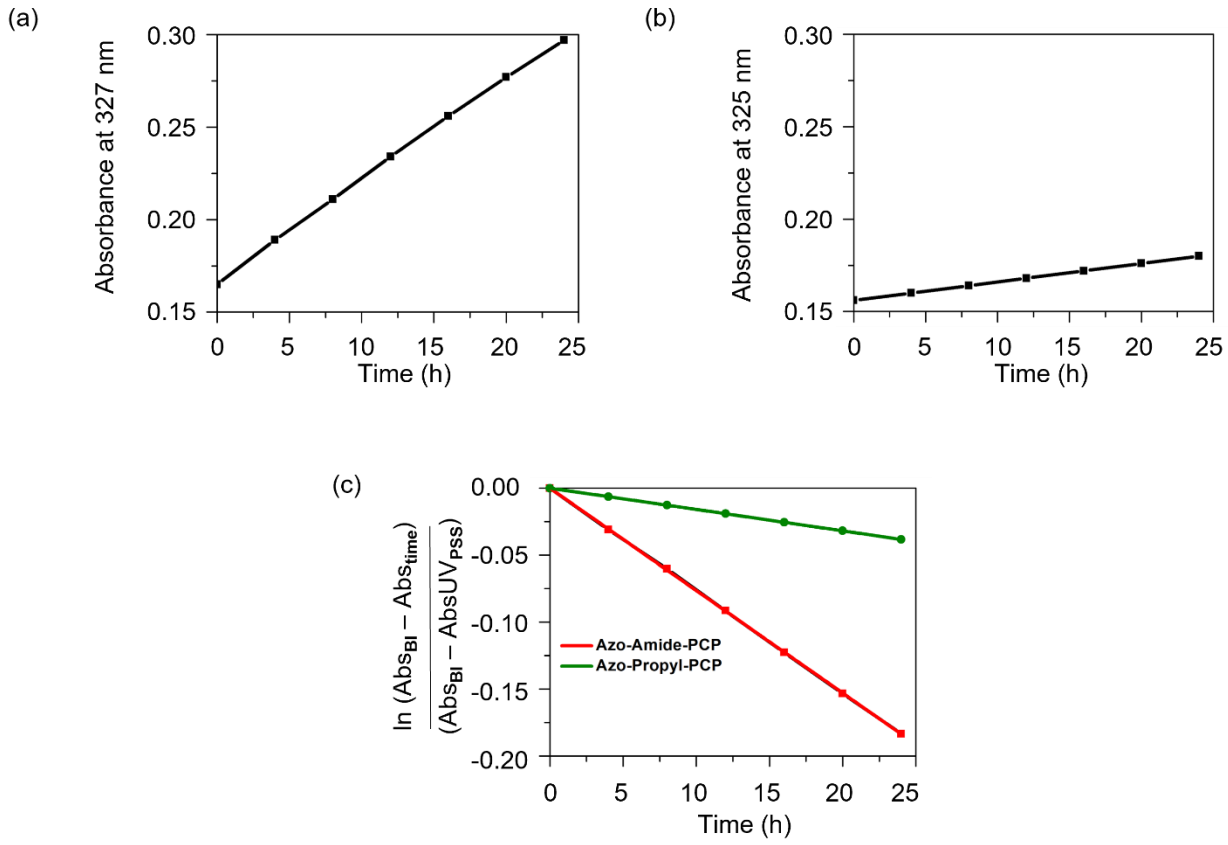

Figure 4. Time course absorbance changes due to thermal back *cis–trans* isomerization of Azo-Amide-PCP (5.93 x 10^{-4} M) (a), Azo-Propyl-PCP (4.73 x 10^{-4} M) (b) in BRB-80 buffer (pH 6.9) after UV_{PSS} at 25°C. The plot showing the rate of thermal back isomerization calculated using the equation, $\ln\left(\frac{(Abs\ (BI) - Abs\ (time)}{Abs(BI) - Abs(UVPSS)}\right) = -kt$, Absorbances at before irradiation (Abs (BI)), at UV photostationary state (Abs (UV_{PSS}), at different time interval (Abs (time)) (c). Rate constant k = 0.0076 h^{-1} ($t_{1/2}$ = 91 h) for Azo-Amide-PCP and k = 0.0016 h^{-1} ($t_{1/2}$ = 430 h) for Azo-Propyl-PCP

Table 1. *cis/trans* ratio of photoresponsive ATP antagonists.

ATP antagonists	UV_{PSS}		Vis_{PSS}	
	cis	*trans*	*cis*	*trans*
AzoTP[25]	92%	8%	29%	71%
Azo-Amide-PCP	92%	8%	28%	72%
Azo-Propyl-PCP	88%	12%	25%	75%

2.2.2 AzoTP and Azo-Amide-PCP molecules in microtubule-dynein *in vitro* motility assay and Basal ATPase assay of AzoTP by cytoplasmic dynein

Next, I investigated the effect of the compounds in the biological activity of dynein motor using an in vitro microtubule gliding assay in a flow cell. In this method, I used a fluorescently labelled (ATTO-647N) microtubules to visualize (excitation at 633nm and the emission maximum at 669nm) their gliding motility on cytoplasmic dynein (single motor unit)-coated glass surface. In sharp contrast to our previous observation of AzoTP-triggered gliding motion of microtubules or actin filaments on kinesin or myosin filaments-coated glass surface, respectively, AzoTP did not trigger microtubule gliding motion with dynein (Figure 5). Even after UV (360 nm)/ Vis (430 nm) light irradiations to the flow cell containing dynein and AzoTP, I did not see any gliding motion of microtubules. These results indicate that dynein behaves differently towards AzoTP-powered

filament motion compared to kinesin and myosin, presumably due to the complex structure and powering mechanism of dynein.

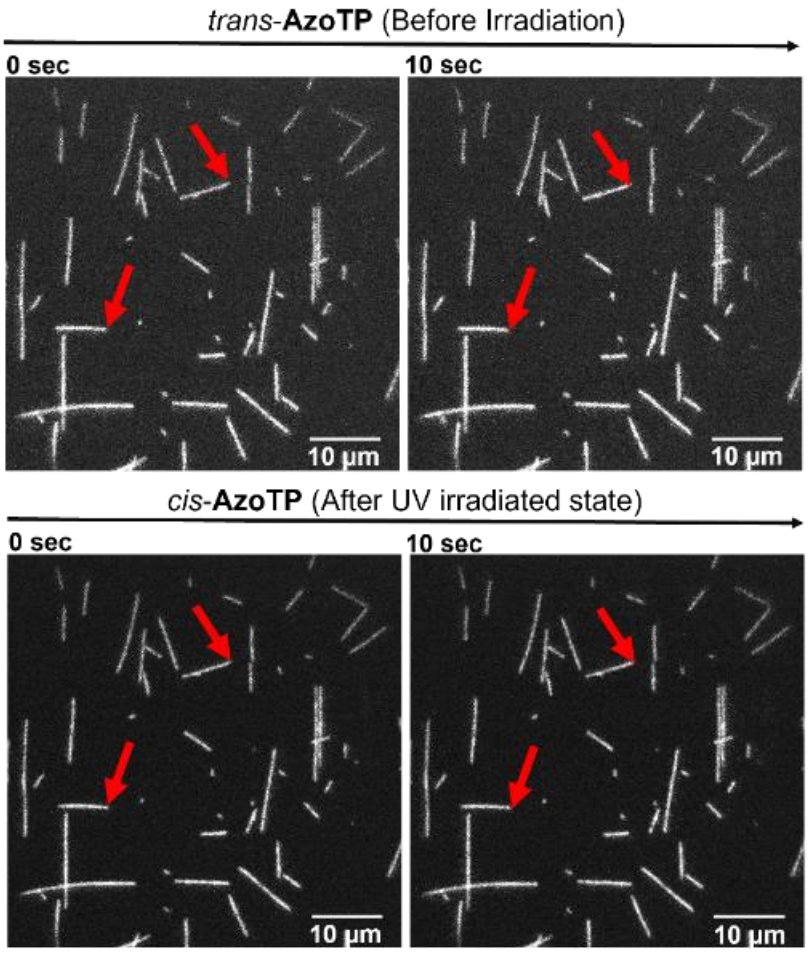

Figure 5. Fluorescence microscopy images of the microtubules obtained at 0 s and 10 s before and after UV irradiation to the flow cell containing AzoTP (1.0 mM). Red arrow indicates the position of the same microtubule at 0 s and 10 s with no significant changes.

To check the inhibitory behavior of AzoTP, I performed the microtubule gliding assay in a flow cell containing dynein, ATP (0.1 mM) and varying amounts of AzoTP (0–10 mM). In this case, ATP in the system can drive the microtubule gliding motion, however I observed a significantly decreased gliding velocity upon increasing the amount of AzoTP (Figure 6a–c). For instance, the

gliding velocity at 5 mM of AzoTP (0.02 μm s^{-1}) was ~20-times lower than that of without AzoTP (0.39 μm s^{-1}). K_i value obtained by fitting the experimental data using Michaelis-Menten equation assuming the competitive inhibition of AzoTP was 531 μM. Then I examined the photoinduced isomerization of AzoTP on the microtubule gliding velocity. Figure 6b shows the fluorescence images of gliding microtubule at 0 and 60 s before and after UV/ Vis light irradiations. At UV_{PSS}, the microtubule gliding velocity was 6.5-times higher (0.13 μm s^{-1}) than that of before irradiation (0.02 μm s^{-1}). At Vis_{PSS}, the gliding velocity became similar to that of before irradiation.

I also checked the ATP hydrolysis activity of dynein using enzyme linked inorganic phosphate assay. In this assay, the absorbance at 360 nm is directly proportional to inorganic phosphate released as a result of ATP hydrolysis. Interestingly, in the presence of dynein, AzoTP (100 μM) exhibited a higher rate of phosphate release (AzoTP: K_m = 65 μM, V_{max} = 3.4 s^{-1}) compared to ATP (100 μM) (K_m = 1.91 μM, V_{max} = 0.32 s^{-1})[30] in a concentration dependent manner (Figure 6d). These results of the motility and hydrolysis experiments suggest that AzoTP occupy the recognition site for ATP in dynein in a competitive manner and capable of undergoing hydrolysis, however the hydrolysis reaction was uncoupled with the motility.[31] Such function as an antagonist against ATP is intrinsically different depending on *trans* and *cis* isomers of AzoTP. Similar photoswitchable inhibitory behavior was also observed when we use Azo-Amide-PCP in the presence of ATP (50 μM) (Figure 6e) (K_i = 1.9 mM). Alternate UV and Vis irradiations were resulted in the reversible switching of microtubule gliding velocity (Figure 6f). I also confirmed that Azo-Propyl-PCP shows a similar inhibition and photoswitching properties like AzoTP and Azo-Amide-PCP in the motility experiments. However, observed some precipitate in buffer solutions containing Azo-Propyl-PCP that could affect the velocity of microtubules. So, I did not evaluate the inhibition property of Azo-Propyl-PCP quantitatively.

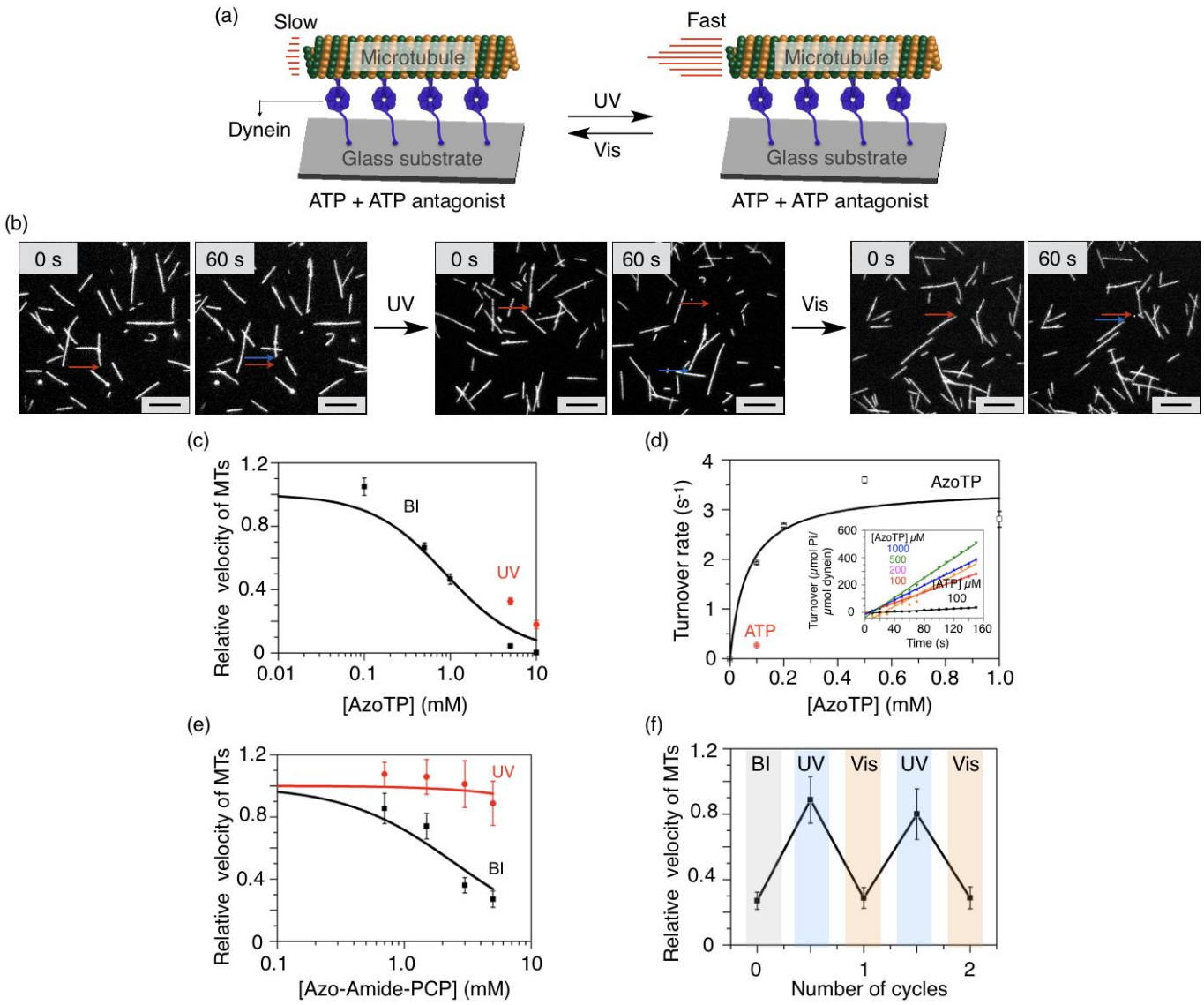

Figure 6. Schematic representation of the dynein-driven microtubule motility on a glass substrate in the presence of ATP and ATP antagonists (a). Florescence microscopy images of the microtubules obtained at 0 s and 60 s after UV and Vis irradiations (AzoTP) Scale bars: 10 μm Red and blue arrows indicate the position of the same microtubule at 0 s and 60 s, respectively (b). Relative gliding velocity of microtubules (MTs) before and after UV/Vis light irradiations in the presence of AzoTP. Error bars represent the standard deviation of 10 microtubules in a single flow cell (c). Turnover of phosphate (Pi) release due to ATP or AzoTP hydrolysis by dynein at time 0–160 s (inset). Error bars represent the standard error (d). Relative

gliding velocity of microtubules (MTs) before and after UV/Vis light irradiations in the presence of Azo-Amide-PCP. Error bars represent the standard deviation of 10 microtubules in a single flow cell (e). Reversible switching in the velocity of MTs over 2 cycles of Azo-Amide-PCP (5 mM; [ATP] = 50 μM) treated sample before (BI) and after UV/Vis light irradiations (f).

2.2.3 Reversible regulation of axonemal dynein activities in *Chlamydomonas* system by Azo-Amide-PCP and Azo-propyl-PCP and control experiments with light

Then, I investigated the effect of ATP antagonists for the control of dynein motor activity in a eukaryotic organism. *Chlamydomonas reinhardtii* is a biflagellar single-cell green algae having dynein motors at its outer and inner arms of the flagella. In *C. reinhardtii*, a cooperative action of multiple dynein motors triggered by ATP produces propulsive force for the beating motion of its flagella.[32-34] I used a uniflagellar mutants of *C. reinhardtii*, which is known to undergo rotational motion.[35–36] To study the effects of ATP antagonists on the behavior of *C. reinhardtii*, the demembranated model was prepared according to the previous studies. [37] I first treated *C. reinhardtii* with a detergent solution to remove its cell membrane, transferred to reactivation buffer containing ATP and observed under an inverted microscope. The resulting demembranated cell exhibited active rotational motion in the presence of ATP (Figure 9). However, the rotational motion was inhibited when ATP antagonist (Azo-Amide-PCP or Azo- Propyl-PCP) present in the reactivation solution (Figure 7 and Figure 8). Interestingly, the rotational motion of *Chlamydomonas* cell restarted after direct UV irradiation (360 nm, 5 s) to the experimental system. Subsequent Vis irradiation (430 nm, 7 s) inhibited the rotational motion cell again (see microscopy images in Figure 7a). The author measured the angle change with respect to the center of the rotating cell and found a significant difference in the values before (0.03 rad. s^{-1}) and after UV irradiation (6.53 rad. s^{-1}) (Azo-Amide-PCP) (Figure 7c). The rate again decreased significantly

after Vis irradiation (0.19 rad. s^{-1}). I optimized the concentration of Azo-Amide-PCP that show maximum inhibition (99% at 1.25 mM) of the cell rotation with reversible photoswitching characteristics (Figure 7d,e).

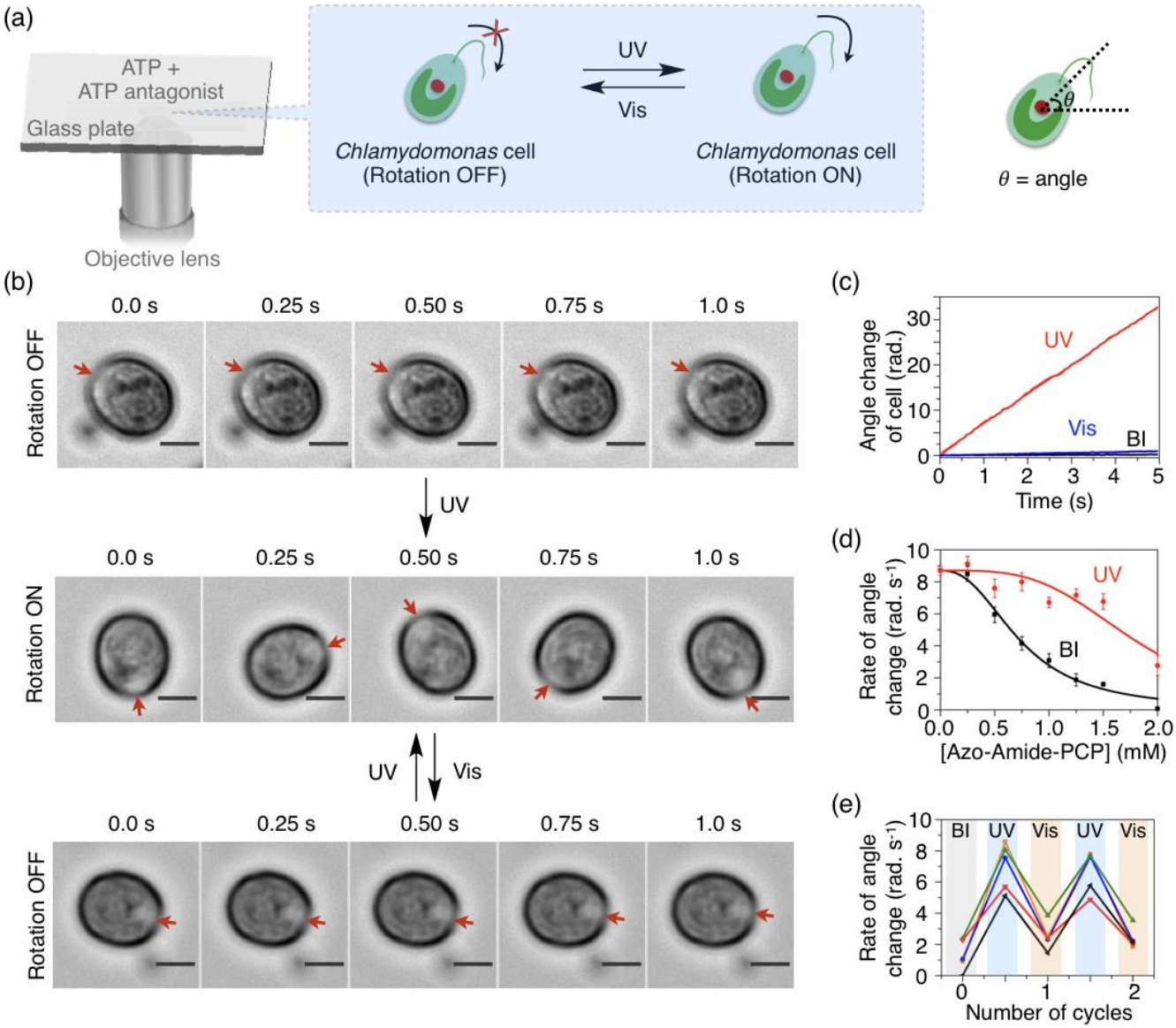

Figure 7. Simplified scheme of experimental condition used for the microscopy imaging of a mutated *Chlamydomonas* cell before and after UV/Vis light irradiations (a). Optical microscopy images showing the rotational motion of the *Chlamydomonas* cell at time 0–1.0 s before and after UV (5 s)/Vis (7 s) light irradiations to the chamber containing Azo-Amide-PCP (1.25 mM) and ATP (100 μM) (b). Scale bars: 5

μm. (red arrows head indicate the reference point of the cell rotation). Graph showing the angle change of *Chlamydomonas* cell at time 0–5 s (c), the rate of angle change of the cell with different concentrations of Azo-Amide-PCP (d), and the reversible switching in the rate of angle change of 5 different cells (black, red, blue, orange and green lines) over 2 cycles before (BI) and after UV/Vis light irradiations (e). Error bars represent the standard error of 8–10 *Chlamydomonas*.

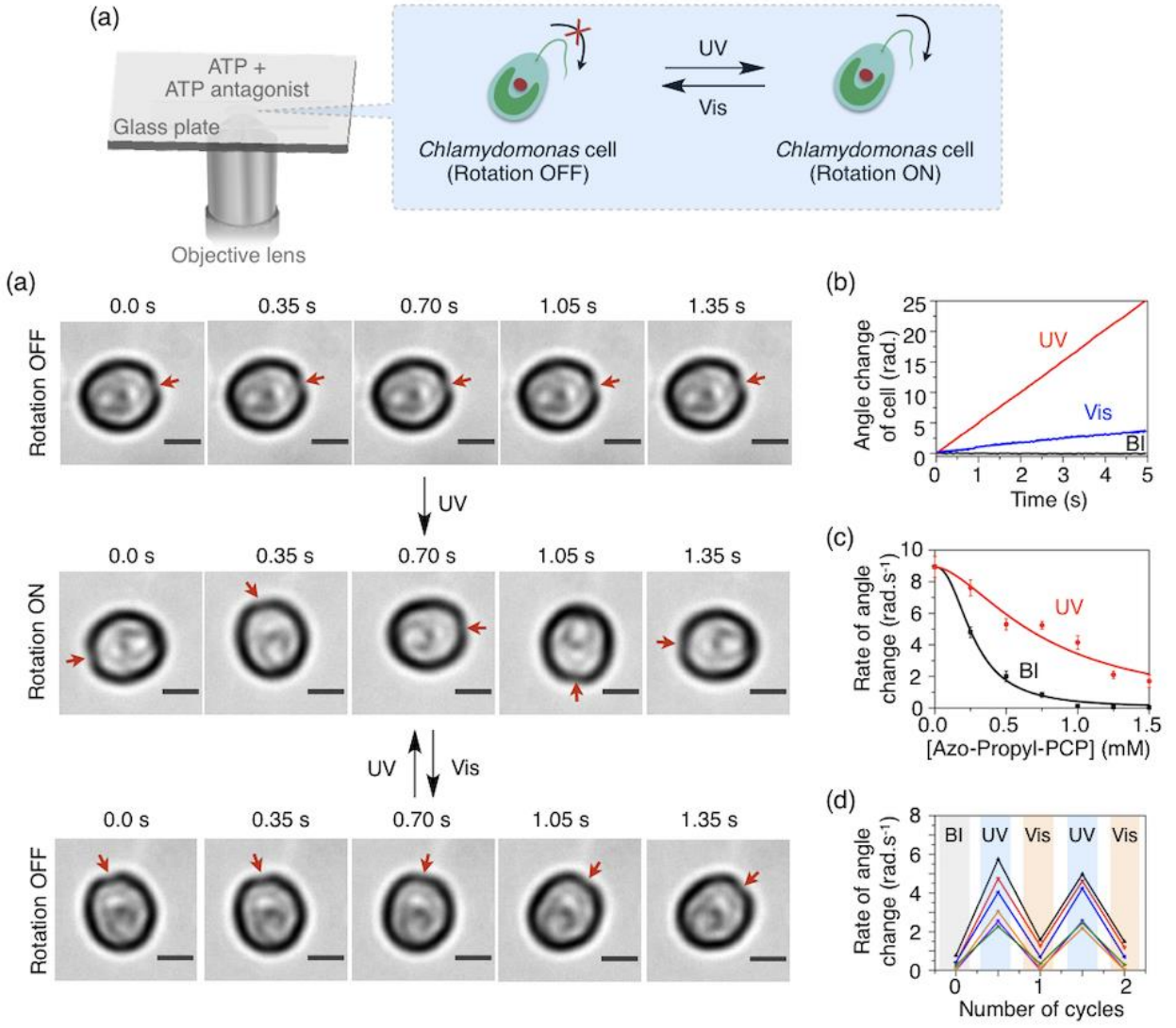

Figure 8. Optical microscopy images showing the rotational motion of the *Chlamydomonas reinhardtii* cell at time 0–1.35 s before and after UV (5 s)/Vis (7 s) light irradiations to the flow cell containing Azo-Propyl-PCP (1.0 mM) and ATP (100 μM) (a). Scale bars: 5 μm. (red arrows head indicate the reference point of the cell rotation. Graph showing the rate of angle change of the cell with different concentrations of Azo-

Propyl-PCP (K_m = 0.14 ± 0.04 mM).[2] (b), the angle change of *Chlamydomonas* cell at time 0–5 s (c), and the reversible switching in the rate of angle change of 6 different cells (black, red, blue, orange, purple and green lines) over 2 cycles before (BI) and after UV/Vis light irradiations (d). Error bars represent the standard error of 8–10 cells.

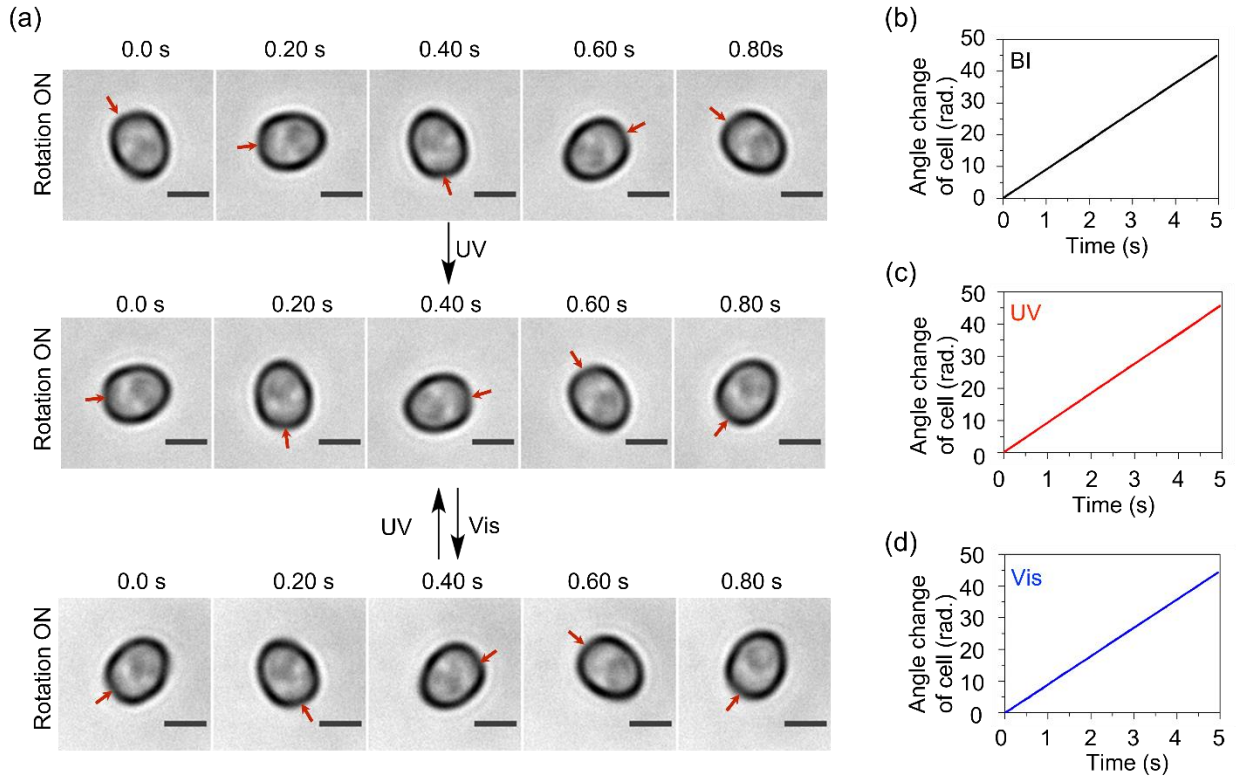

Figure 9. Optical microscopy images of the *Chlamydomonas reinhardtii* cell at time 0–0.8 s before and after UV (5 s)/Vis (7 s) light irradiations to the flow cell containing ATP (100 µM) without ATP antagonists (a). Scale bars: 5 µm. Red arrows head indicate the reference point of the cell rotation. Graph showing the angle change of *Chlamydomonas* cell at time 0–5 s before (b) and UV (c)/Vis (d) light irradiations. Repeated UV/Vis light irradiation without ATP antagonists showed no significant effect on the rotational motion *Chlamydomonas* cell. The rate of angle change was 9.1 ± 0.007 rad. s^{-1} (BI), 9.18 ± 0.095 rad. s^{-1} (UV_{PSS}) and 8.95 ± 0.005 rad. s^{-1} (Vis_{PSS}).

Similar reversible switching of the rate of angle change was also observed in the case of Azo-Propyl-PCP (BI; 0.01 rad. s^{-1}, UV; 5.07 rad. s^{-1} and Vis (0.71 rad. s^{-1}) (Figure 8). I checked the effect of UV/Vis irradiations for the rotational motion of cell without ATP antagonists and found no inhibitory behavior (Figure 9). These results indicate that ATP antagonist present in the experimental system plays an important role for the reversible inhibition of *Chlamydomonas* cell rotation, presumably via binding with axonemal dyneins. The K_i values obtained by fitting the experimental data of Azo-Amide-PCP were 0.27 mM (*trans*) and 4.73 mM (*cis*) while those of Azo-Propyl-PCP were 0.03 mM (*trans*) and 0.36 mM (*cis*). The difference in K_i values between *trans* and *cis* isomers of ATP antagonists further indicates that the ATP antagonists preferably bind to dynein in *trans* isomer than their *cis* isomer.

2.2.4 Computational docking studies of Azo-triphosphates with the motor domain of cytoplasmic dynein

The author studied molecular docking to know the ATP antagonist binding with the receptors of dynein using AutoDock Vina. The cytoplasmic dynein protein structure from protein data bank (3VKG) was used as the ATP receptor model.[38] Figure 10 shows the docked ligands in the ATP binding site of dynein (AAA1 chain) superimposed with the docked *trans*/*cis*-AzoTP and *trans*/*cis*-Azo-Amide-PCP. Azobenzene motif of the ATP antagonists in its *trans* isomer showed a parallel orientation with the adenine motif of ATP, however *cis* isomer was in perpendicular orientation. This result indicates the shape incompatibility of ATP antagonist in their *cis* isomer. Binding affinity of *trans* and *cis* isomers docked ATP antagonist further indicate the less affinity of *cis* isomers to the binding site than *trans* isomers (Figure 10b).

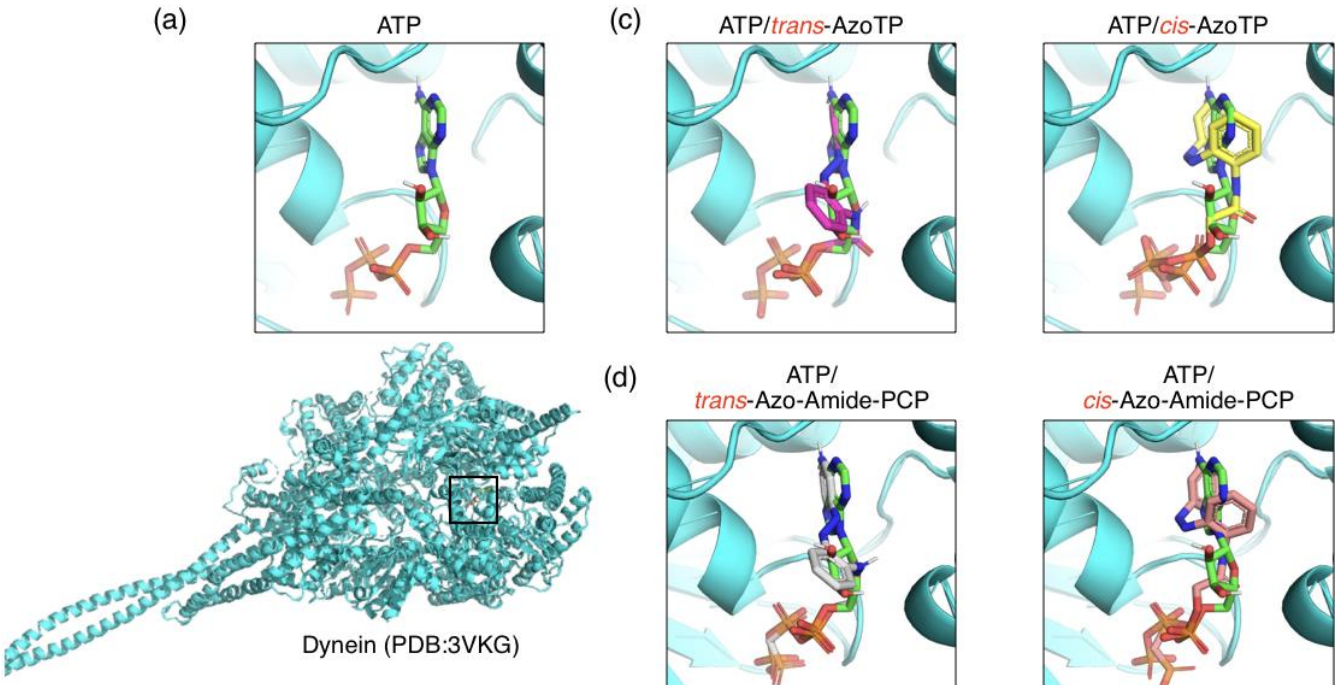

(b)

Docked ligands (chain AAA1)	Binding energy (kcal/mol)
ATP	-9.4
trans-AzoTP	-8.9
cis-AzoTP	-7.6
trans-Azo-Amide-PCP	-9.1
cis-Azo-Amide-PCP	-7.6
trans-Azo-Propyl-PCP	-8.9
cis-Azo-Propyl-PCP	-8.1

Figure 10. Scheme showing the docked ligands in the ATP binding site of cytoplasmic dynein (AAA1 chain; PDB 3VKG) (a). Table showing the binding energy of docked ligands (b). The ligand ATP in the binding site of dynein AAA1 chain superimposed with the docked *trans*/*cis*-AzoTP (c), *trans*/*cis*-Azo-Amide-PCP (d) and *trans*/*cis*-Azo-Propyl-PCP (e).

2.3 Experimental Section

2.3.1 Chemicals

All chemicals and biochemical reagents were purchased from commercial sources (Merck; Wako Pure Chemical industries; Tokyo Chemical industries; Kanto Chemicals, Thermo Fisher Scientific) and used without further purification.

2.3.2 General methods, instrumentation, and measurements

JEOL (ECX-400) spectrophotometer was used to measure NMR spectra (^{1}H, ^{13}C, ^{31}P). Purity analysis of the synthesized Azo-Amide-PCP and Azo-Propyl-PCP molecules were performed by using the Shimadzu reversed-phase (RP) HPLC system. Freeze drying of the compounds was done by using an EYELA FDU-2200 lyophilization system. High-resolution mass spectroscopy analysis was performed by Thermo Scientific Exactive mass spectrometer with electron spray ionization (ESI). Chromatographic purification was performed using silica gel 60 N (neutral, 6-120 µm, Kanto chemicals). Absorption spectra were recorded by Shimadzu UV-1800 spectrophotometer. Thin-layer chromatography was performed on precoated silica gel 60 F_{254} aluminum sheets (MERCK). Asahi Spectra CL-1503 LED controller and Hamamatsu LED controller were used for 430 nm and 365 nm light for photoisomerization studies and reversible modulation of the activities of dynein in *in vitro* motility assay.

2.3.3 Synthesis scheme

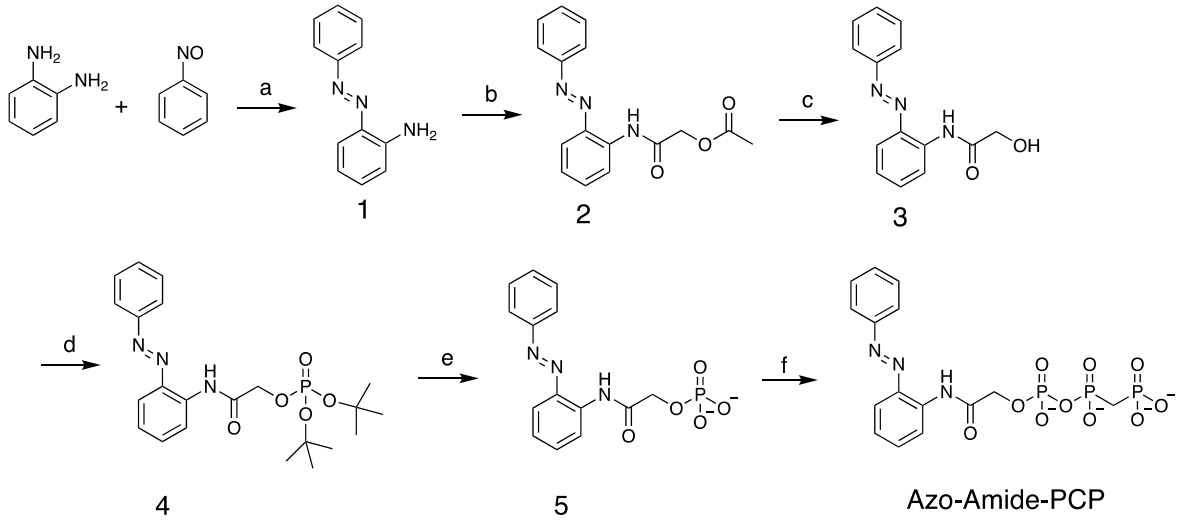

Reagent and condition: (a) AcOH, toluene, N_2, 60 °C, 24 h; (b) Acetoxyacetyl chloride, Triethylamine, DCM, r.t, 1 h.; (c) K_2CO_3, MeOH, RT, overnight. (d) di-*tert*-butyl *N*,*N*-diisopropylphosphoramidite, 1*H*-tetrazole, dry THF, Ar, r.t, 7 h; then, mCPBA, 0 °C, 1h; then rt, 40 min; (e) trifluoroacetic acid, dry CH_2Cl_2, Ar, r.t, 6 h; then eluting through DEAE Sephadex A-25 anion exchanger, TEAB; (f) tributylamine, carbonyldiimidazole, tributylammonium, methylenediphosphate, dry DMF, Ar, rt, overnight.

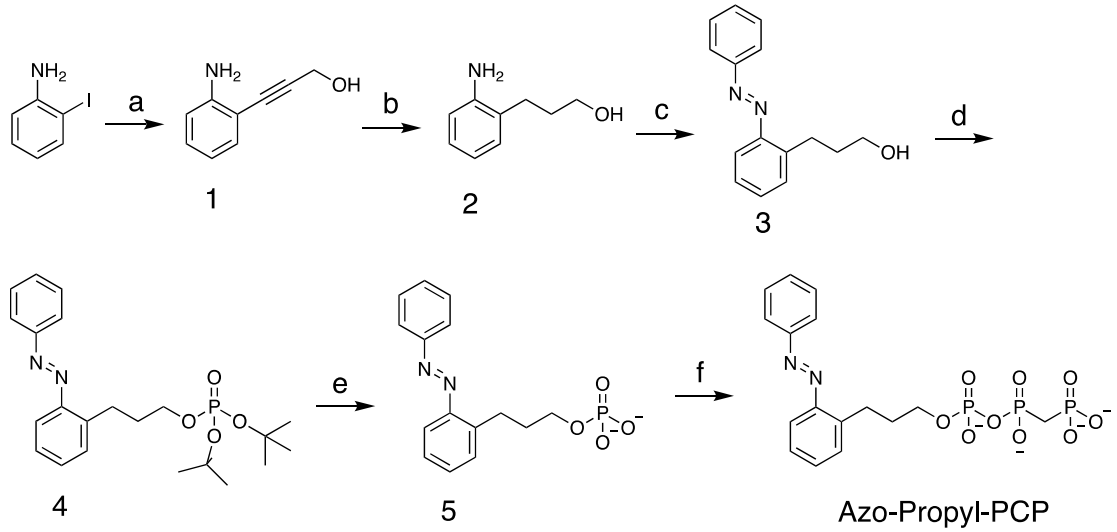

Reagent and condition: (a) CuI, bis(triphenylphosphine)palladium(II) dichloride, 2-propyn-1-ol, triethylamine, r.t, 18 h. (b) 10% Pd/C, H_2, MeOH, RT, 48 h. (c) Nitrosobenzene, AcOH, toluene, N_2, 60 °C, 21 h. (d) Di-tert-butyl N,N-diisopropylphosphoramidite, 1H-tetrazole, dry THF, Ar, r.t, 6 h, then mCPBA, 0 °C, 1 h. (e) TFA, dry DCM, Ar, RT, 6 h. (f) Tributylamine, carbonyldiimidazole, tributylammonium methylenediphosphonate, dry DMF, Ar atmosphere, r.t, overnight.

General synthetic procedure for the monophosphate into triphosphate conversion

First, a solution of methylenediphosphonic acid (6.5 eq) in (2 ml) of water was added dropwise to a flask containing tributylamine (2 eq) at 4 °C with vigorous shaking. The solvent was evaporated at 30 °C room temperature with dry-MeOH (3 x 30 mL) to prepare tributyl ammonium methylenediphosphonate and dried under vacuum.

Then, tributyl ammonium salt of compound **5** was prepared by mixing compound **5** in dry MeOH with tributylamine (3.3 eq) followed by the solvent evaporation. The crude mixture obtained was dissolved in dry DMF and added a solution of 1,1'- carbonyldiimidazole (6.3 eq) in dry DMF under Ar at room temperature. After 16 h, dry MeOH (0.2 eq) was added and stirred for another 1 h to quench the excess 1,1'- carbonyldiimidazole. Then, the reaction mixture was added dropwise to a dry DMF solution of above prepared tributyl ammonium methylenediphosphonate. After 12 h, the reaction mixture was cooled to 0 °C in an ice bath, added cold water and pH adjusted to 7.5 using 1 M NaOH. Diethyl ether was added to the reaction mixture, the compound extracted in water and the aqueous phase was evaporated with EtOH at 30°C and dried under vacuum. The residue was dissolved in 0.2 M triethyl-ammonium hydrogen carbonate (TEAB), applied to DEAE-Sephadex A-25 column (2.5x 30 cm, 10 g), and eluted with a linear gradient (0.2M-1.0M; total volume; 1L) of TEAB solution (over 400 min) at 4 °C. The target elution fraction was

collected and evaporated with EtOH at 30°C several times to remove TEAB buffer and dried under vacuum. The obtained residue was redissolved in dry MeOH (2 ml). Then, a 1 M NaI in acetone (5 ml) was added to above mixture where the sodium salt of the target compound precipitated. The precipitate was filtered and washed with acetone several times followed by lyophilization.

Azo-Amide-PCP (Yield. 65%): ^{1}H NMR (400 MHz, D_2O) δ 8.01 – 7.94 (m, 3H), 7.73 (d, *J* = 8.1, 1H), 7.66 – 7.60 (m, 4H), 7.43 (t, *J* = 7.4 Hz, 1H), 4.67 (d, *J* = 7.3 Hz, 2H), 2.35 (t, *J* = 20.4 Hz 2H), ^{13}C NMR (100 MHz, D_2O, CD_3OD as the standard) δ 171.36 (d, *J* = 9.3 Hz), 153.14 (s), 144.27 (s), 134.92 (s), 133.54 (s), 133.08 (s), 130.64 (s), 127.69 (s), 124.99 (s), 123.85 (s), 118.14 (s), 65.63 (s), 28.90 (d, *J* = 5.6 Hz).). ^{31}P NMR (160 MHz, D_2O (H_3PO_4) as the external standard) δ 15.69 (d, *J* = 8.6 Hz), 8.42 (dd, *J* = 25.9, 8.6 Hz), -11.94 (d, *J* = 25.9 Hz). HR-MS (ESI, m/z) calculated for $C_{15}H_{15}N_3Na_4O_{10}P_3$ $[M+H]^+$: 581.95556; found: 581.95581.

Azo-Propyl-PCP (yield 61%): ^{1}H NMR (400 MHz, D_2O) δ 7.94 (dd, J = 8.0, 1.8 Hz, 2H), 7.66–7.48 (m, 6H), 7.42-7.38 (m, 1H), 3.99 (q, J = 6.6 Hz, 2H), 3.20 (t, J = 7.9 Hz, 2H), 2.28 (t, J = 20.6 Hz, 2H), 1.97 (quin, J = 7.9 Hz, 2H). ^{13}C NMR (100 MHz, D_2O, CD_3OD as the standard) δ 153.31 (s), 151.44 (s), 141.84 (s), 132.67 (d, *J* = 7.8 Hz), 132.03 (s), 130.58 (s), 128.22 (s), 123.59 (s), 116.75 (s), 66.86 (d, *J* = 5.9 Hz), 33.18 (d, *J* = 7.5 Hz), 30.32 (d, *J* = 7.0 Hz), 28.19 (s). ^{31}P NMR (160 MHz, D_2O (H_3PO_4) as the external standard) δp 14.64 (d, *J* = 8.3 Hz), 8.32 (dd, *J* = 25.7, 7.9 Hz), -10.54 (d, *J* = 25.7 Hz). HR-MS (ESI, m/z) calculated for $C_{16}H_{18}N_2Na_4O_9P_3$ $[M+H]^+$: 566.98104; found: 566.98235.

2.3.4 Characterization of Azo-Amide and Azo-Propyl PCP molecules (HPLC, NMR, and ESI-Mass)

Purity analysis of Azo-Amide-PCP and Azo-Propyl-PCP by reverse-phase HPLC

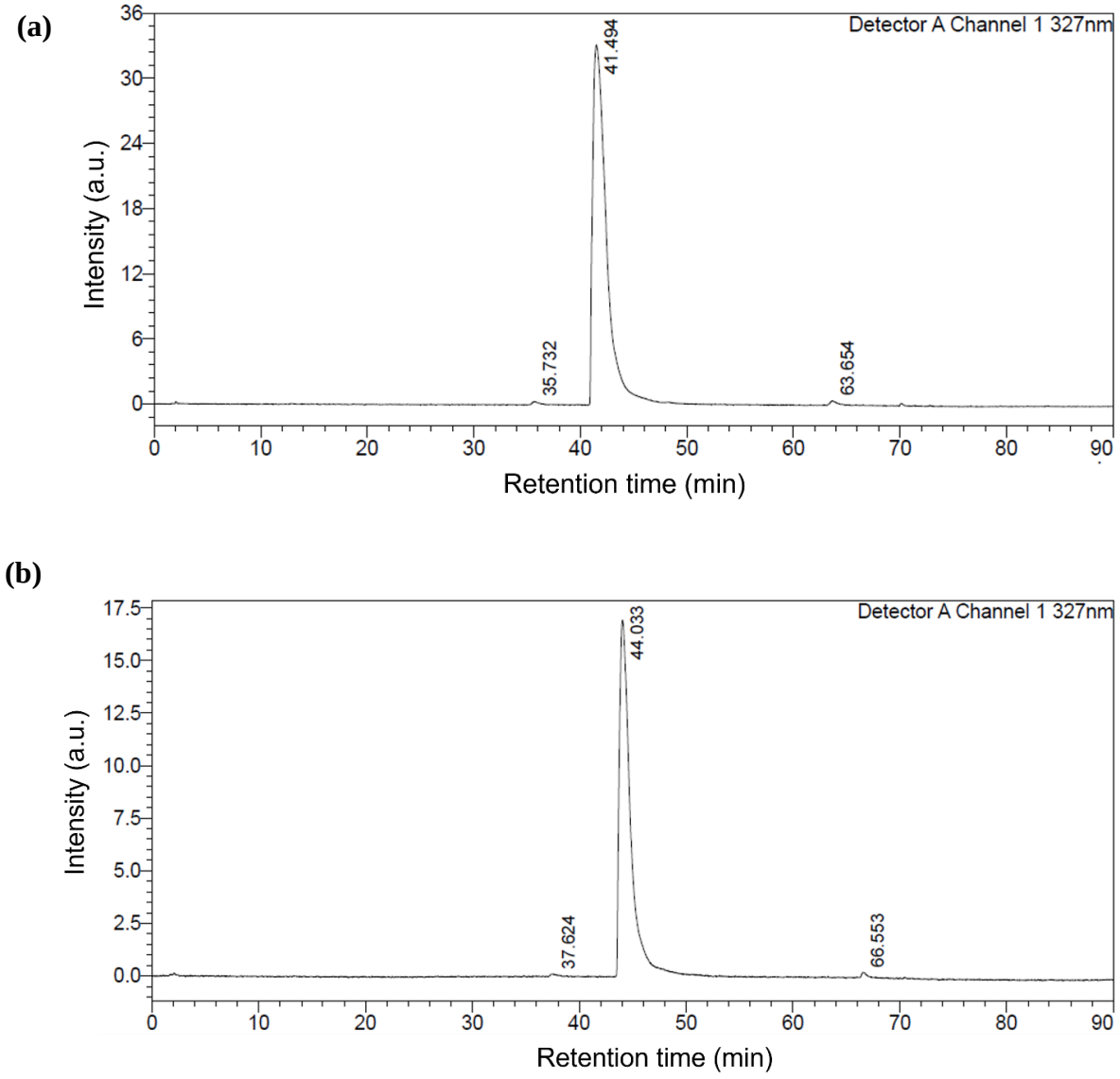

Figure 1.Reverse phase HPLC chromatograms (detection wavelength 327 nm, flow rate: 1.0 mL/min, room temperature) of **Azo-Amide-PCP** (a) and **Azo-Propyl-PCP** (b) that show > 96 % purity. 10–70 % of CH_3CN in sodium phosphate buffer (pH 6) used as eluent with Mightysil column (RP-18 GP (L) 150 x 4.6, 5µm, Kanto Chemical).

NMR spectral data.

^{1}H NMR ^{13}C NMR and ^{31}P spectra of Azo-Amide-PCP

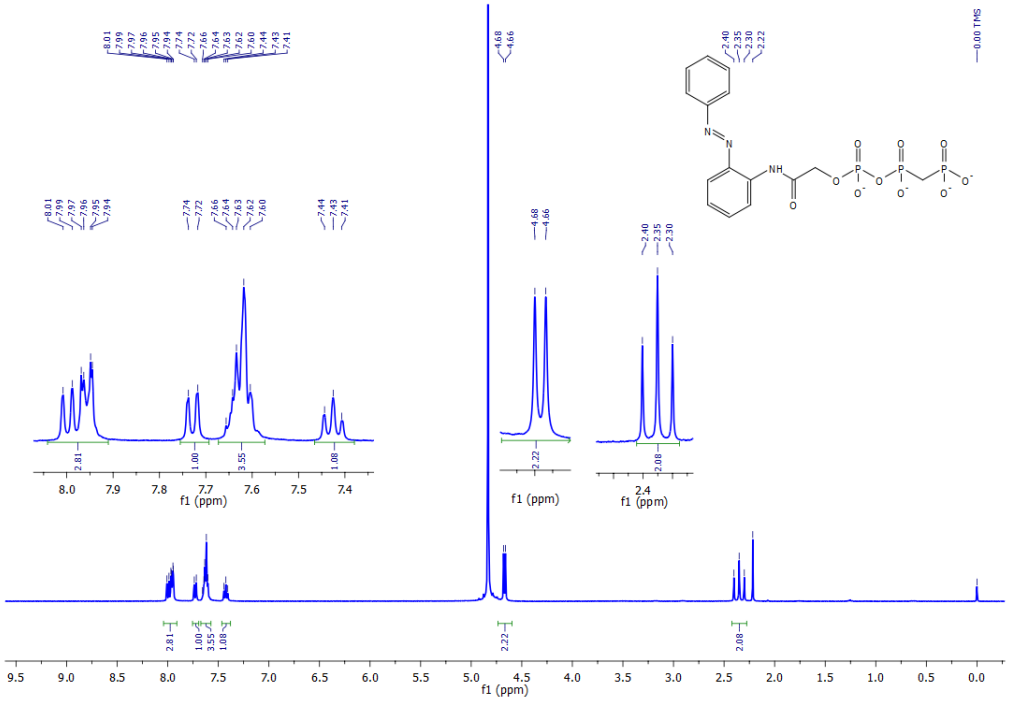

Figure 2. ^{1}H NMR of Azo-Amide-PCP

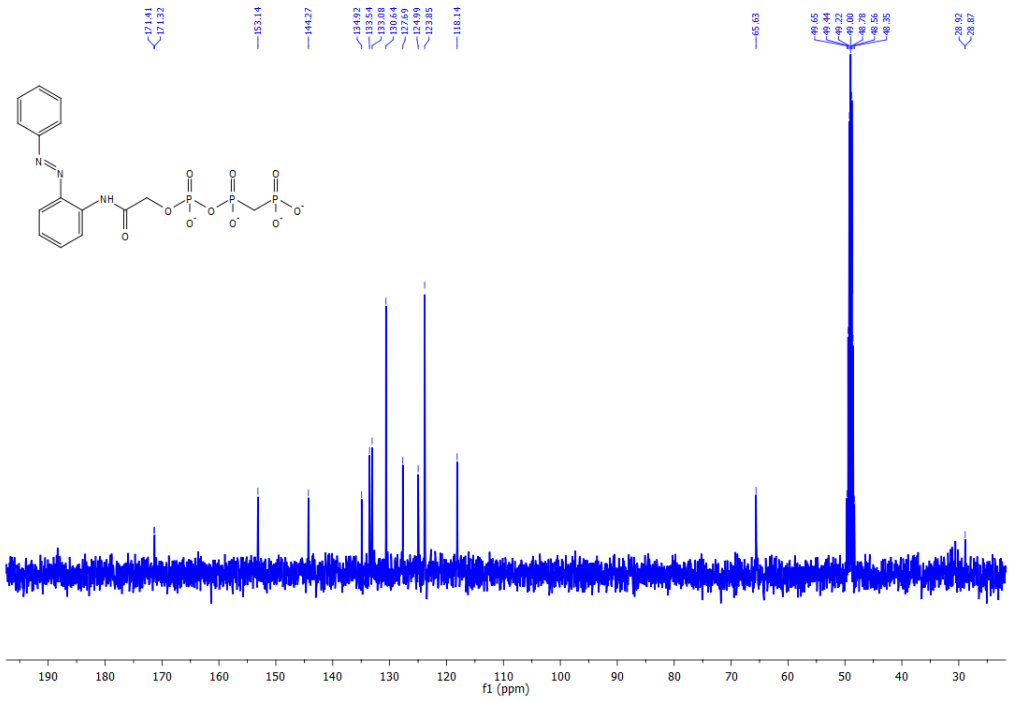

Figure 3.^{13}C NMR of Azo-Amide-PCP

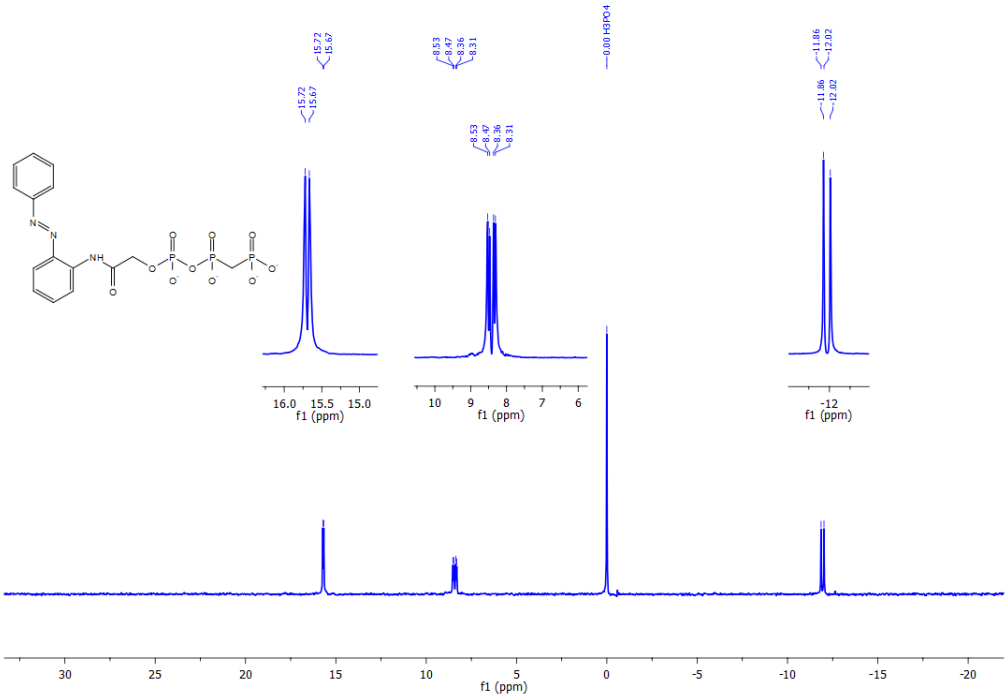

Figure 4. ^{31}P NMR of Azo-Amide-PCP

^{1}H NMR ^{13}C NMR and ^{31}P spectra of Azo-Propyl-PCP

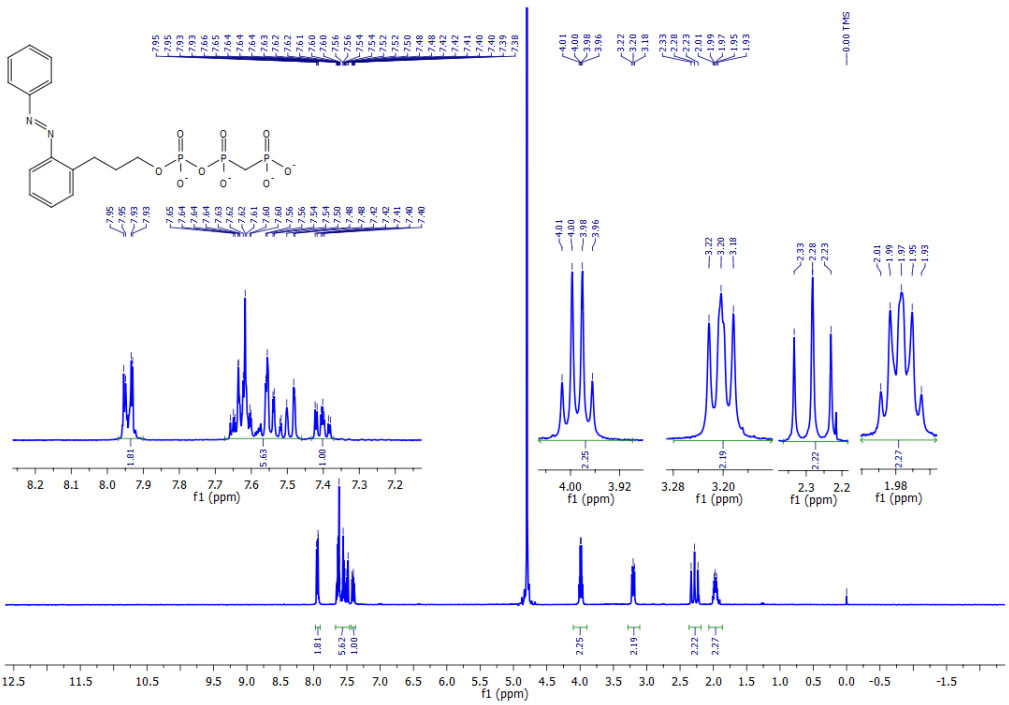

Figure 5. ^{1}H NMR of Azo-Propyl-PCP

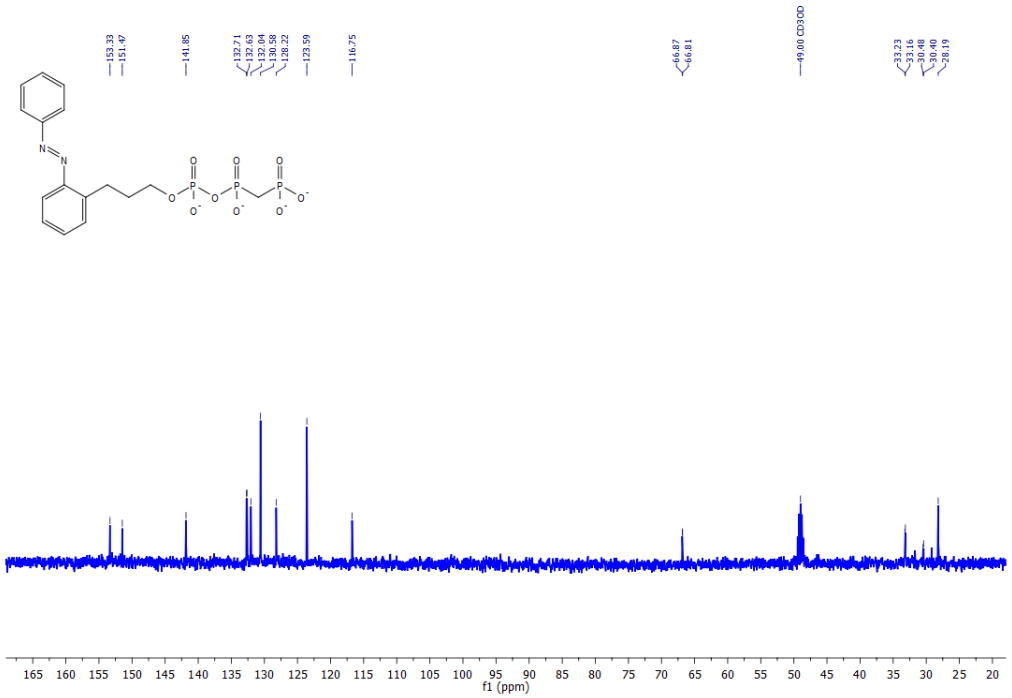

Figure 6. ^{13}C NMR of Azo-Propyl-PCP

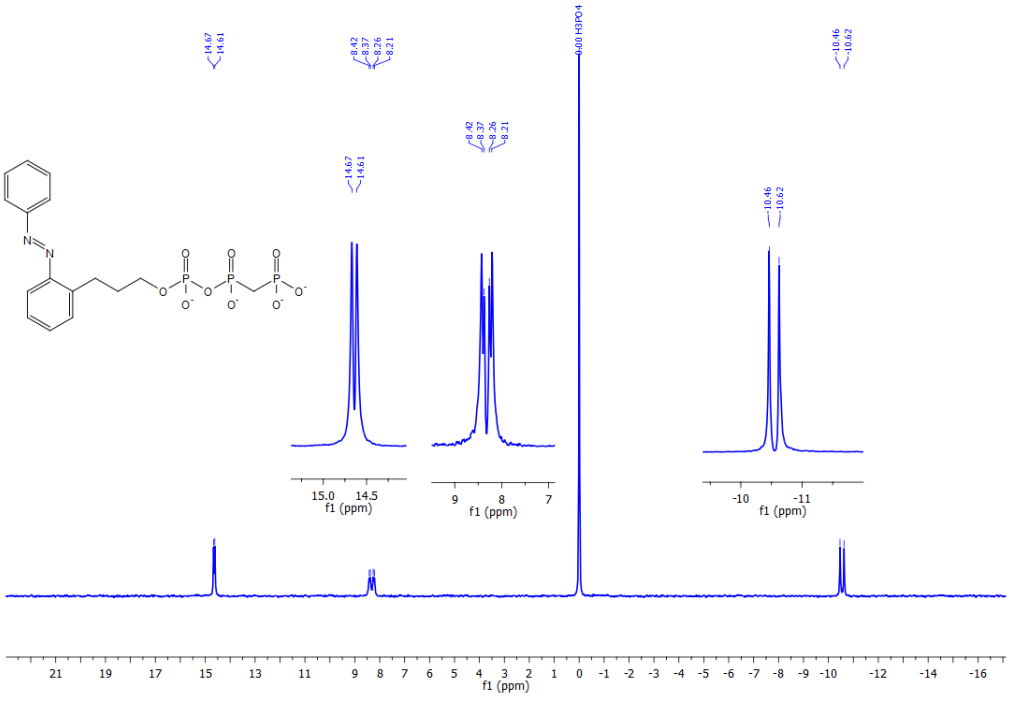

Figure 7. ^{31}P NMR of Azo-Propyl-PCP

High resolution mass spectra of Azo-Amide-PCP and Azo-Propyl-PCP

(a)

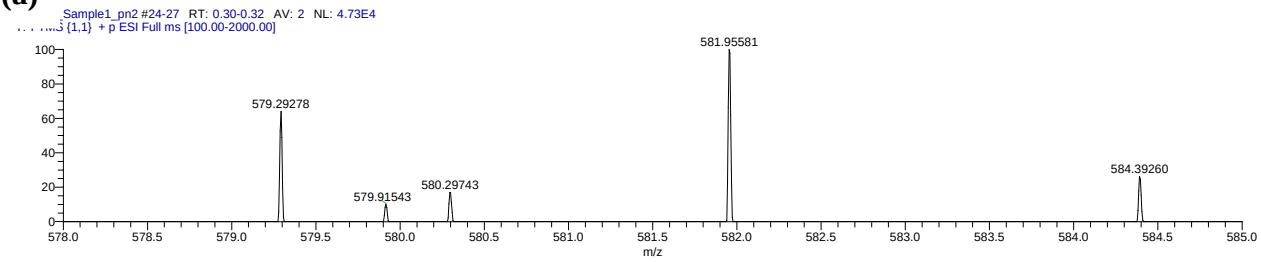

Azo-Amide-PCP. Calculated for $C_{15}H_{15}N_3Na_4O_{10}P_3$ [M-H] $^+$: 581.95556; found: 581.95581.

(b)

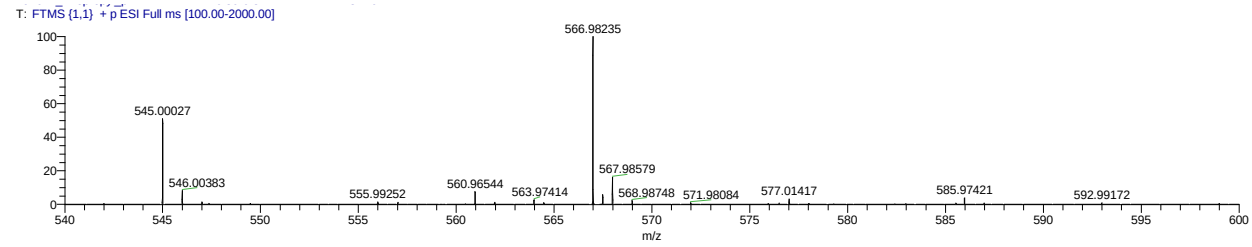

Azo-Propyl-PCP. Calculated for $C_{16}H_{18}N_2Na_4O_9P_3$ [M-H] $^+$: 566.98104; found: 566.98235.

Figure 8. High-resolution mass spectra

2.3.5 Preparation of recombinant human cytoplasmic dyneins

The recombinant human cytoplasmic dynein construct (monomeric) was prepared as His8-SBP-FLAG-BioEase-DHC1(1306–4646) in the pcDNA3.4 plasmid vector.[30] The construct was transiently expressed in the Expi293 cells, purified via two-step affinity chromatography using Ni-IMAC resin (156–0133, Bio-Rad), and anti-FLAG agarose (A2220, Sigma-Aldrich).

2.3.6 Preparation of tubulin and fluorescently labelled microtubules

Tubulin was prepared according to the methods described previously.[40] Briefly, tubulin was purified from porcine brain through two successive cycles of polymerization and depolymerization using a high molarity PIPES buffer method. An aliquot of tubulin was

labelled with ATTO 647N NHS ester (AD 647N-31, ATTO-TEC). The yield of the labelling was ca. 19%. To prepare fluorescently labelled microtubules, ATTO 647-tubulins were copolymerized with unlabeled tubulin at a ratio of 1:5 for 30 min at 37 °C in the presence of 1mM GTP in BRB80 (80 mM PIPES-KOH pH 6.8, 1 mM EGTA, and 1 mM $MgCl_2$) and stabilized with 40 μM paclitaxel (T1912, Sigma-Aldrich).

2.3.7 Dynein-microtubule *in vitro* motility assay

Microtubule gliding on cytoplasmic dynein-coated surface was observed in the presence of ATP and various ATP antagonists at 24 ± 1 °C, according to the method described previously with slight modifications.[39] Briefly, the space formed between two coverslips (18×18 mm^2 #C218181 and 24×32 mm^2 #MGCS001E7, thickness No.1; Matsunami Glass) with the spacer of two slivers of Parafilm (Heathrow Scientific LLC) was used as a flow cell.[40] Heating the flow cell at 100 °C on the hot plate for few seconds melted the Parafilm and the film sealed tightly the coverslips together. The resultant flow cell has approximate dimensions of 2.5 mm in width, 18 mm in length and 150 μm in height.

The flow cell was filled with 7 μL of 2 mg/mL biotinylated BSA (A6043, Sigma-Aldrich) in BRB80 buffer and incubated for 3 min at room temperature. The flow cell was washed with 35 μL of BRB80 buffer and then incubated with 7 μL of 1 mg/mL streptavidin (Type II, 192–11641, Wako; filtered with a 0.1 μm spin filter before use) in 10 mM PIPES-KOH pH 6.8. After 3-minute incubation, the flow cell was filled with 21 μL of 7 mg/mL casein (07319-82, Nacalai) in casein buffer (25 mM HEPES-NaOH, pH 8.6, 50 mM K-acetate) and incubated for 3 min at room temperature. The flow chamber then was filled with 7 μL of 45 μg/mL dynein construct in buffer A (25 mM imidazole pH 8.0, 25 mM KCl, and 4 mM $MgCl_2$) for 3 min at room temperature. After washing with 21 μL of buffer A, 21 μL

of Gliding buffer (25 mM imidazole pH 8.0, 25 mM KCl, 6 mM $MgCl_2$, 0.7 mg/mL casein, 100 μM ATP, 0.218 mg/mL glucose oxidase, 0.04 mg/mL catalase, 2 mM dithiothreitol, 10 μM paclitaxel, and 25 mM glucose) including ca. 4 μg/mL fluorescent microtubules was introduced into the flow cell and then washed with Gliding buffer without microtubules. Microtubule gliding was imaged using a custom-built, objective-type total internal reflection fluorescence microscope based on Ti-E (Nikkon) equipped with an oil immersion objective lens (CFI Apochromat TIRF 60XC Oil, NA/1.49). The fluorescence dye was excited using a 632.8-nm He-Ne laser (Model 30991, 5 mW, Research Electro Optics Inc.). A dichroic mirror (FF640-FDi01-25x36, Semrock) and a bandpass filter (FF01-676/29, Semrock) were used. The fluorescence image was detected by an EMCCD camera (iXon Life 897, Andor). The following equation was used for fitting (K_m value of ATP[41] = 152 ± 18 μM, [S] = 50 or 100 μM).

$$v = (K_m + [S])/(K_m(1 + [I]/K_i) + [S]).$$

Relative velocity = v/v_0 , where v_0 is the velocity in the absence of an inhibitor.

2.3.8 Measurement of steady-state ATPase

Steady-state ATPase activities of dynein in the presence of ATP antagonists were measured using the EnzChek Phosphate Assay Kit (Life Technologies). The absorbance at 360 nm was monitored by the SYNERGY H1 microplate reader (BioTEK) every 10 s for 10 min at 25°C. Assays were performed in reaction buffer (10 mM PIPES-KOH at pH 6.8, 25 mM potassium acetate, 4 mM $MgSO_4$, 1 mM EGTA, 20 μM taxol, 200 μM 2-amino-6-mercapto-7-methylpurine riboside and 1 U/ml purine nucleoside phosphorylase) containing 100 nM dynein and 100 μM ATP, or various concentrations of antagonists (0.1- 1 mM).

2.3.9 *Chlamydomonas reinhardtii* cell culture

Chlamydomonas reinhardtii strain uni-1, was grown in TAP medium at 25° C in light/dark cycles (12 h /12 h).[37] 15 ml of cell suspension in the mid-log phase was centrifuged at 1000 × g for 3 min. The obtained cell pellet was washed twice with Milli Q and a wash buffer (10 mM HEPES, 0.5 mM EGTA, pH 7.4). For demembranation, 0.25 mL (5 volume of cell pellet) of an ice-chilled aqueous solution (30 mM HEPES, 5 mM $MgSO_4$, 1 mM DTT, 1 mM EGTA, 50 mM K-acetate, 1% (w/v) polyethylene glycol [20,000 mol wt] and 0.1 % Nonidet P-40) was added to the cell pellet (50 μL) and incubated for 5 min at 25°. The suspension was gently mixed to avoid flagella loss. Then, 10 μL of demembranated cells suspension was diluted with 200 μL of the above aqueous solution. For reactivation, 10 μL of the diluted solution was mixed with 10 μL of reactivation solution with 200 μM ATP. All the experiments after demembranation were performed at 0° C except for the microscopy observation.

2.3.9.1 Microscopy observation of the cell rotation

The plasma-treated cover glass (Matsunami no.1, 24x50 mm) was coated with 20 μL of 2% (w/v) MPC polymer (Lipidure-CM5206; NOF Corporation) in ethanol. The cover glass was heated at 50° C for 30 min to dry ethanol. The observation solution containing the demembranated cells was placed into a chamber made by a silicone sheet (thickness of 1 mm) with a hole 4mm diameter sandwiched between the MPC coated glass and a cover glass (Matsunami no.1, 18x24 mm). The cells in the demineralized cell suspension placed in the holes of the silicon sheet were observed in red light (M700L4, 700nm; Thorlabs) under an inverted microscope (IX 73; Olympus) using an objective lens (LUCPlan 40x, NA 0.6; Olympus) equipped with a CMOS camera (ORCA-Flash4.0; Hamamatsu). The video recording speed was set to 20 FPS. Fiji (https://imagej.net/software/fiji/) was used to

analyze the angle change of the cells at BI and after irradiation of UV (365 nm)/Vis (430 nm) light. The cells ten seconds after/before irradiation were used for analysis. The movement of the cells for five seconds was used to obtain the angle change. The following equation was used for fitting the experimental data (see **2.9.3** details).

$$v_{\mathrm{i}} = v_0\,(K_{\mathrm{m}} + [\mathrm{S}])/(K_{\mathrm{m}}(1 + [\mathrm{I}]^n/K_{\mathrm{i}}) + [\mathrm{S}])$$

2.3.9.2 Molecular docking

The binding site of ADP in chain A near to LEU1947 was chosen as the docking site. Only polar hydrogen atoms were added to the model, and then the input PDBQT file of the receptor was generated by using AutoDockTools (1.5.6).[42] The 3D models of all the ligands were generated with their SMILES strings by using eLBOW program in Phenix software suite.[43] Then, AutoDockTools merged the non-polar hydrogen atoms and set up the rotatable bonds to create the input PDBQT file of candidate ligands. A grid box with the size of (16Å, 22Å, 16Å) centered at (x=76 Å, y=138 Å, z=68Å) was set up for the docking simulation which was performed by using Autodock Vina(1.1.2).[44]

2.3.9.3 Normalized equation for fitting the *Chlamydomonas* experimental data

Based on the observation of the less-efficient inhibition effect at lower inhibitor concentration in the cell experiment, we set a cooperative inhibition model as shown by the following reaction for the analysis of *Chlamydomonas* rotational activity at different concentration of ATP antagonists.

$$\begin{array}{l} \mathrm{E} + \mathrm{S} \underset{k_{-1}}{\overset{k_1}{\rightleftharpoons}} \mathrm{ES} \xrightarrow{k_2} \mathrm{E} + \mathrm{P} \\ + \\ \mathrm{nI} \\ \Big\uparrow\!\!\Big\downarrow k_{\mathrm{i}} \\ \mathrm{EI_n} \end{array}$$

where E, S, I, P, and n are dynein, ATP, ATP antagonists as inhibitors, ADP with phosphate, and the number of inhibitors attaching the dynein. The rate constants of each reaction are k_1, k_{-1}, and

k_2. The dissociation constant between dynein and ATP becomes $K_{\mathrm{m}} = [\mathrm{E}_0][\mathrm{S}_0]/[\mathrm{ES}_0]$, and the total concentration of dynein is $[\mathrm{E}_{\mathrm{t}0}] = [\mathrm{E}_0] + [\mathrm{ES}_0]$, in which subscript 0 means the absence of ATP antagonists. Using these equations, the concentration of the dynein-ATP complex becomes $[\mathrm{ES}_0] = [\mathrm{E}_{\mathrm{t}0}][\mathrm{S}_0]/(K_{\mathrm{m}} + [\mathrm{S}_0])$. Then, in the presence of the inhibitor, the dissociation constant for dynein and ATP is $K_{\mathrm{m}} = [\mathrm{E}][\mathrm{S}]/[\mathrm{ES}]$, and the dissociation constant for dynein and inhibitor is $K_{\mathrm{i}} = [\mathrm{E}][\mathrm{I}]^n/[\mathrm{EI}_n]$. In this condition, the total amount of enzymes is $[\mathrm{E}_{\mathrm{t}}] = [\mathrm{E}] + [\mathrm{EI}_n] + [\mathrm{ES}]$. Using these equations, the concentration of the dynein-ATP complex becomes $[\mathrm{ES}] = [\mathrm{E}_{\mathrm{t}}][\mathrm{S}]/([\mathrm{S}] + (1 + [\mathrm{I}]^n/K_{\mathrm{i}})K_{\mathrm{m}})$. When the reaction rates in the presence and absence of ATP antagonists are expressed as $v_{\mathrm{i}} = k_2[\mathrm{ES}]$ and $v_0 = k_2[\mathrm{ES}_0]$, respectively, their ratio becomes $v_{\mathrm{i}}/v_0 = [\mathrm{ES}]/[\mathrm{ES}_0]$. In this experiment, the dynein concentration is constant regardless of the presence or absence of ATP antagonists. The amount of free ATP is also considered almost constant under these conditions to be regarded as $[\mathrm{E}_{\mathrm{t}}] = [\mathrm{E}_{\mathrm{t}0}]$ and $[\mathrm{S}] = [\mathrm{S}_0]$. Therefore, the rate of dynein activity will be $v_{\mathrm{i}} = v_0\,(K_{\mathrm{m}} + [\mathrm{S}])/([\mathrm{S}] + (1 + [\mathrm{I}]^n/K_{\mathrm{i}})K_{\mathrm{m}})$. In our analysis, we used this equation to evaluate the angle change of the demembranated *Chlamydomonas*. The n represents the cooperativity of ATP analogs for dynein, and higher the value means higher the cooperativity. By fitting the experimental data to the equation, n of Azo-Amide-PCP were 2.4 (*trans*) and 3.6 (*cis*) while those of Azo-Propyl-PCP was 2.3 (*trans*) and 1.67 (*cis*). The cooperativity of Azo-Amide-PCP for binding to dynein is higher in the *cis*-isomer. In comparison, the cooperativity of Azo-Propyl-PCP is higher in the *trans* isomer.

2.4 Conclusions

In conclusion, author successfully developed azobenzene-based ATP antagonists that show a reversible control of motor activity of isolated cytoplasmic dynein as well as axonemal dynein of a eukaryotic organism. Using an *in vitro* microtubule motility assay, we demonstrated that the ATP antagonists can inhibit the gliding motion of microtubule, however, regain the motion by UV light irradiation. The reversible photoisomerization of ATP antagonists between *trans* and *cis* isomers lead the reversible photoswitching of the microtubule gliding motility. The ATP antagonists also showed the inhibition of the axonemal dynein activity for force generation in a demembranated model of *Chlamydomonas reinhardtii*. The rotational motion of *Chlamydomonas* cell was inhibited in the presence of ATP antagonists, however reverted rapidly by UV irradiation, and alternate UV/Vis irradiations resulted in the reversible switching of the rotational motion of *Chlamydomonas* cell. The *trans* and *cis* isomers of ATP antagonists significantly differ in their affinity to the ATP binding site of cytoplasmic dynein.

2.5 References

[1] P. Mitchell, *Science*, **1979**, *206*, 1148–1159

[2] G.M Cooper, *The cell: A molecular approach*. 2nd edition, **2000**, Sinauer Associates, Sunderland (MA).

[3] M. Regnier, D.M Lee, and E. Homsher, *Biophys J.* **1998**, *74*, 3044–3058.

[4] M. Kinoshita, *Biophysics and Physicobiology*, **2021**, *18*, 60–66.

[5] R. D. Vale, *Cell*, **2003**, *112*, 467–480.

[6] H J Agteresch, P C Dagnelie, J W van den Berg, and J H Wilson, *Drugs*, **1999**, *58*, 211–232.

[7] S.M Gilbert, C.J Oliphant, S. Hassan, A.L Peille, P. Bronsert, S. Falzoni, F. Di Virgilio, S. McNulty, and R. Lara, *Oncogene*, **2019**, *38*, 194–208.

[8] I. M. Welleman, M. W. H. Hoorens, B. L. Feringa, H. H. Boersma and W. Szymanski. *Chem. Sci.*, **2020**, *11*, 11672–11691.

[9] A. A. Beharry and G. A. Woolley, *Chem. Soc. Rev.*, **2011**, *40*, 4422–4437.

[10] H. M. D. Bandara and S. C. Burdette, *Chem. Soc. Rev.*, **2012**, *41*, 1809–1825.

[11] T. Seki, *Bull. Chem. Soc. Jpn.*, **2018**, *91*, 1026–1057.

[12] M. Kathan and S. Hecht, *Chem. Soc. Rev.*, **2017**, *46*, 5536–5550.

[13] D. M. Barber, S. A. Liu, K. Gottschling, M. Sumser, M. Hollmann and D. Trauner, *Chem. Sci.*, **2017**, *8*, 611–615.

[14] M. Schehr, C. Ianes, J. Weisner, L. Heintze, M. P. Müller, C. Pichlo, J. Charl, E. Brunstein, J. Ewert, M. Lehr, U. Baumann, D. Rauh, U. Knippschild, C. Peifer and R. Herges, *Photochem. Photobiol. Sci.*, **2019**, *18*, 1398–1407.

[15] I. R. Gibbons, *Cell Motil. Cytoskeleton*, **1995**, *32*, 136–144.

[16] B. M. Paschal and R. B. Vallee, *Nature*, **1987**, *330*, 181–183.

[17] P. Höök and R. B. Vallee, *J. Cell Sci.*, **2006**, *119*, 4369–4371

[18] G. Bhabha, H. C. Cheng, N. Zhang, A. Moeller, M. Liao, J. A. Speir, Y. Cheng and R. D. Vale, *Cell*, **2014**, *159*, 857–868.

[19] T. Kon, M. Nishiura, R. Ohkura, Y. Y. Toyoshima and K. Sutoh, *Biochemistry*, **2004**, *43*, 11266–11274.

[20] T. Kon, T. Oyama, R. Shimo-Kon, K. Imamula, T. Shima, K. Sutoh and G. Kurisu, *Nature*, **2012**, *484*, 345–350.

[21] S. Karki and E. L. Holzbaur, *Curr. Opin. Cell Biol.*, **1999**, *11*, 45–53.

[22] R. B. Vallee, J. C. Williams, D. Varma and L. E. Barnhart, *J. Neurobiol.*, **2004**, *58*, 189–200.

[23] I. R. Gibbons *J. Cell Biol.*, **1981**, *91*, 107–124.

[24] L. M. DiBella and S. M. King, *Int. Rev. Cytol.*, **2001**, *210*, 227–268.

[25] N. Perur, M. Yahara, T. Kamei and N. Tamaoki, *Chem. Commun.*, **2013**, *49*, 9935–9937.

[26] H. M. Menezes, M. J. Islam, M. Takahashi and N. Tamaoki, *Org. Biomol. Chem.*, **2017**, *15*, 8894–8903.

[27] M. J. Islam, K. Matsuo, H. M. Menezes, M. Takahashi, H. Nakagawa, A. Kakugo, K. Sada and N. Tamaoki, *Org. Biomol. Chem.*, **2019**, *17*, 53–65.

[28] D. Samanta, J. Gemen, Z. Chu, Y. Diskin-Posner, L. J. W. Shimon and R. Klajn, *Proc. Natl. Acad. Sci. U. S. A.*, **2018**, *115*, 9379–9384.

[29] J. Volaric, W. Szymanski, N. A. Simeth, and B. L Feringa, *Chem. Soc. Rev.*, **2021**, *50*, 12377–12449.

[30] R. Ibusuki, T. Morishita, A. Furuta, S. Nakayama, M. Yoshio, H. Kojima, K. Oiwa, and K. Furuta. *Science*, **2022**, *375*, 1159-1164.

[31] T. Shimizu, *J. Biochem.*, **1987**, *102*, 1159–1165.

[32] O. Kagami and R. Kamiya, *J. Cell Sci.*, **1992**, *103*, 653–664.

[33] J. Lin and D. Nicastro. *Science* **2018**, *360*, eaar1968.

[34] S. Toba, H. Iwamoto, S. Kamimura and K. Oiwa, *Biophys. J.*, **2015**, *108*, 2843–2853.

[35] C.J. Brokaw, D.J.L. Luck, and B. Huang, *J. Cell Biol.*, **1982**, *92*, 722–732.

[36] Huang B, Ramanis Z, Dutcher SK, and Luck DJ, *Cell.*, **1982**, *29*, 745-753.

[37] R. Kamiya and G. B. Witman, *J. Cell Biol.*, **1984**, *98*, 97–109.

[38] T. Kon, T. Oyama, R. Shimo-Kon, K. Imamula, T. Shima, K. Sutoh, and G. Kurisu. *Nature*, **2012**, *484*, 345–350.

[39] A. Furuta, M. Amino, M. Yoshio, K. Oiwa, H. Kojima and K. Furuta. *Nat. Nanotechnol*, **2017**, *12*, 233–237.

[40] M. Castoldi, A. V. Popov. *Protein Expr. Purif.* **2003**, *32*, 83–88.

[41] T. Torisawa, M. Ichikawa, A. Furuta, K. Saito, K. Oiwa, H. Kojima, Y.Y. Toyoshima, K. Furuta. *Nat. Cell Biol*, **2014**, *16*, 1118–1124.

[42] G. M. Morris, R. Huey, W. Lindstrom, M. F. Sanner, R. K. Belew, D. S. Goodsell, and A. J. Olson. *J. Computational Chemistry*, **2009**, *16*, 2785–2791.

[43] P. D. Adams, P. V. Afonine, G. Bunkóczi, V. B. Chen, I. W. Davis, N. Echols, J. J. Headd, L.-W. Hung, G. J. Kapral, R. W. Grosse-Kunstleve, A. J. McCoy, N. W. Moriarty, R. Oeffner, R. J. Read, D. C. Richardson, J. S. Richardson, T. C. Terwilliger and P. H. Zwart. *Acta Cryst. D*, **2010**, *66*, 213–221.

[44] O. Trott and A. J. Olson. *Journal of Computational Chemistry*, **2010**, *31*, 455–461.

Chapter 3
Conclusion of the thesis

In this dissertation work, the author developed azobenzene-based photoswitchable ATP antagonists for controlling the activity of motor proteins; cytoplasmic and axonemal dyneins. The new ATP antagonists showed reversible photoswitching of cytoplasmic dynein activity in an *in vitro* dynein-microtubule system due to the *trans* and *cis* photoisomerization of their azobenzene segment. Importantly, the new ATP antagonists reversibly regulated the axonemal dynein motor activity for the force generation in a demembranated model of *Chlamydomonas reinhardtii*. The photoresponsive change in the motor activity is well explained by molecular docking studies and found that the *trans* and *cis* isomers of ATP antagonists significantly differ in their affinity to the ATP binding site. The author, envisioned that, this data shows the power of a reversible photoregulatory tool in controlling the function of biological motor in a dynamic manner. Taking advantage of the high spatiotemporal precision of photochromic system, the interesting next step is to apply the ATP antagonists for specific macroscopic function in living animal.

List of publications

1. Sampreeth Thayyil, Yukinori Nishigami, Md. Jahirul Islam, P.K. Hashim, Ken'ya Furuta, Kazuhiro Oiwa, Jian Yu, Min Yao, Toshiyuki Nakagaki, Nobuyuki Tamaoki, Dynamic control of microbial movement by photoswitchable ATP antagonists, *Chem. Eur. J.*, **https://doi.org/10.1002/chem.202200807**

2. Kazuya Matsuo, Sampreeth Thayyil, Mitsuyasu Kawaguchi, Hidehiko Nakagawa, and Nobuyuki Tamaoki, A visible light-controllable Rho kinase inhibitor based on a photochromic phenylazothiazole, *Chem. Commun*., 2021, 57, 12500-12503.

Acknowledgements

Firstly, I owe my deepest gratitude to the God, for his help and blessings to complete this doctoral course.

This research work is completed first and foremost because of the continuous support and guidance, from my supervisor Professor Nobuyuki Tamaoki. I would like to express my sincere gratitude to him throughout the doctoral research. I gratefully acknowledge the professor Toshiyuki Nakagaki and Assistant professor Yukinori Nishigami (Hokkaido University) for providing the lab facilities to perform experiments and their valuable guidance during the experiments. I would also like to express my gratitude to Assistant professor P.K. Hashim for the help in the preparation of manuscript. I gratefully thank all former and current lab members of Professor Tamaoki lab (2017-2022) for the valuable suggestions and support during the research. I gratefully acknowledge the previous Associate professor Dr. Yuna Kim. and Assistant Professors, Dr. Yoshimitsu Sagara, Dr. Kazuya Matsuo for their kind help and valuable suggestions.

I would like to pay my tribute to Hokkaido University, Japan for giving me the opportunity to study and explore the culture of Japan. I would also like to thank IGP-program for selecting me as MEXT-Scholarship student for conducting the doctoral research.

Last but not least, I would like to thank my mother and father who constantly encourage and supports me throughout the studies.